**Supporting Information**

# Energy Cascaded Upconversion in an Organic Dye-Sensitized Core/Shell Fluoride Nanocrystal

Guanying Chen,[1,2]* Jossana Damasco,[1] Hailong Qiu,[1,2] Wei Shao,[1,2] Tymish Y. Ohulchanskyy,[1] Rashid R. Valiev,[3,4] Xiang Wu,[5] Gang Han,[5] Yan Wang,[1] Chunhui Yang,[1] Hans Ågren[3] and Paras N. Prasad[1,6]*

[1]Institute for Lasers, Photonics, and Biophotonics, University at Buffalo, State University of New York, Buffalo, NY 14260, USA

[2]School of Chemical Engineering and Technology, Harbin Institute of Technology, Harbin, Heilongjiang, 150001, P. R. China

[3]Department of Theoretical Chemistry&Biology, Royal Institute of Technology, S-10691 Stockholm, Sweden

[4]Tomsk State University, 36 Lenin Avenue, 634050, Tomsk, Russian Federation

[5]Department of Biochemistry and Molecular Pharmacology, University of Massachusetts Medical School, Worcester, Massachusetts 01605

[6]Department of Chemistry, Korea University, Seoul, 136-701, Korea

*E-mails: chenguanying@hit.edu.cn; pnprasad@buffalo.edu.

**Table of Contents:**


**A. Chemicals and Instrumentation** 3

**B. Synthetic Procedures** 6

**(Tables S1 and S2, Scheme S1, Figs. S1-S3)**

**C. Sample Preparations** 9

**D. Supporting Figures for Core/Shell Nanostructures** 14

**(Figs. S4-S18, Table S3)**

**E. Supporting Figures for IR Dye-Sensitized Core/Shell Nanostructures** 26

**(Figs. S19-33, Table S4)**

**F. Estimations of Molecular Weights, Number of Dyes per Core/Shell Nanoparticle, and Intermolecular Distance of IR Dye on the Surface of a Core/Shell nanoparticle** 37

**G. Quantification of Upconversion Quantum Efficiency and Pump Power Dependence** 33

**(Figs. S34 and S35)**

**H. Supporting Figures for Generalization of Dye-Sensitized Core/Shell Structure** 41

**(Figs. S36-S39)**

**I. Supporting Figures for Applications** 43

**(Figs. S39 and S40)**

**J. The Theoretical Modeling** 44

**(Figs. S41-45)**

**K. References** 52

# A. Chemicals and Instrumentation

## A1. General Chemicals

Yttrium(III) oxide ($Y_2O_3$, 99.99%), ytterbium (III) oxide ($Yb_2O_3$, 99.9%), thulium (III) oxide ($Tm_2O_3$, 99.99%), erbium (III) oxide ($Er_2O_3$, 99.99%), holmium (III) oxide ($Ho_2O_3$, 99.99%), neodymium (III) oxide ($Nd_2O_3$, 99.99%), lutetium (III) oxide ($Lu_2O_3$, 99.99%), yttrium(III) chloride hexahydrate ($YCl_3$•$6H_2O$, 99.99%), thulium (III) chloride hexahydrate ($TmCl_3$•$6H_2O$, 99.99%), neodymium (III) chloride hexahydrate ($NdCl_3$•$6H_2O$, 99.99%), trifluoroacetic acid ($CF_3COOH$, 99%), sodium trifluoroacetate ($CF_3COONa$, 98%), oleic acid (90%, tech grade), oleylamine (70%, tech grade) and octadecene (90%, tech grade), IR-783 (dye content 90%), IR 806 (dye content 90%), IR 820 (dye content 80%), Indocyanine green, 4-mercaptobenzoic acid (99%), nitrosonium tetrafluoroborate ($NOBF_4$, 95%), N,N-dimethylformamide (DMF, anhydrous, 99.8% ), dimethyl sulfoxide (DMSO, ≥99.9%), ammonia fluoride ($NH_4F$, ≥99.99% trace metals basis), sodium hydroxide (NaOH, anhydrous, ≥97%), polystyrene (average Mw ~280,000) were obtained from Sigma Aldrich. Methanol (ACS reagent grade, ≥99.8%), hexane (ACS reagent grade, ≥98.5%), and chloroform (ACS reagent grade, ≥99.8%) were purchased from Fisher Scientific. All materials were used as received.

## A2. Instrumentation

***Morphology and Composition.*** The size and morphology of the resulting core/shell nanoparticles were characterized by transmission electron microscopy (TEM) using a JEM-2010 microscope at an acceleration voltage of 200 KV. The powder X-ray diffraction (XRD) patterns were recorded by a Siemens D500 diffractometer, using Cu Kα radiation (λ=0.15418 nm). The 2θ angle of the XRD spectra was recorded at a scanning rate of 5 °/minute. The contents of elements were analyzed with energy-dispersive X-ray spectroscopy (EDX) using a Hitachi SU70 Field Emission Scanning Electron Microscope with Oxford Energy-dispersive X-ray Spectrometer, and quantified with inductively coupled plasma mass spectrometry (ICP-MS) utilizing a Thermo Scientific XSERIES 2 ICPMS Single Quadrupole Mass Spectrometer with Inductively Coupled Plasma Source.

***Absorption and luminescence.*** Absorption spectra of IR dyes, colloidal core/shell nanoparticles, as well as IR dye-sensitized core/shell nanoparticles dispersed in DMF were acquired using a Shimadzu 3600 UV–Visible-NIR spectrophotometer. The upconversion luminescence (UCL) spectra were recorded using a Fluorolog-3.11 Jobin Yvon spectrofluorometer. The UCL signal of the sample in the cuvette was collected at 90° relative to the excitation light. Near infrared (NIR) downconversion luminescence (DCL) spectra were recorded using a SPEX 270M spectrometer (Jobin Yvon) equipped with an InGaAs TE-cooled photodiode (Electro-Optical Systems, Inc.). Laser excitation for PL was provided by a tunable Ti:Sapphire laser (Tsunami from Spectra Physics) operating in free-running (unlocked) mode. All luminescence spectra have been corrected for the spectral sensitivity of the spectroscopy system using the Fluorolog spectrofluorometer calibration curve (for UCL) or NIST-traced calibration light source (HL-2000-CAL-ISP, Ocean Optics) (for DCL).

***Luminescence Decay.*** The luminescence decay profiles at 860 nm from $Nd^{3+}$ ions were recorded with an Infinium oscilloscope (Hewlett-Packard) coupled to the PMT of the Fluorolog-3.11 Jobin Yvon spectrofluorometer. Excitation at 532 nm from a nanosecond pulsed Nd:YAG laser (Lotis TII, Belarus) at a repetition rate of 20 Hz was used for luminescence excitation. The lifetime of fluorescence at ~ 840 nm from the IR dye was measured using a time-correlated single-photon counting (TCSPC) technique. The decay was recorded by an H7422 (Hamamatsu) detector (having a response time in the range of 250 ps) attached to a SPC-830 TCSPC module (Becker & Hickl). A Ti: sapphire laser (Chameleon from Coherent) providing femtosecond (~120 fs) pulses at 750 nm with 76 MHz repetition rate was used as the excitation source. Additional filters in the signal path were used to cut off scattered excitation and select specific fluorescence wavelength range. The SPC Image software (Becker & Hickl) was used for deconvolution and data fitting to evaluate lifetime values. The effective lifetime $\tau_m$ was used when necessary to analyze the decay process, using the following equation,[1]

$$\tau_m = \frac{\int_0^{+\infty} tI(t)dt}{\int_0^{+\infty} I(t)dt} \qquad \text{(S1)}$$

where $I$(t) is the luminescence intensity at time t.

***Luminescence Excitation Spectra.*** A Ti: Sapphire laser (Chameleon from Coherent), which is capable of lasing in a broad wavelength range of 680-1080 nm at a repetition rate of 76 MHz (~120 fs), was tuned with 5-10 nm step to excite the UCL, and the UCL spectra for each laser excitation wavelength was recorded by the Fluorolog-3.11 Jobin Yvon-Horiba spectrofluorometer. The laser power output was adjusted to remain constant throughout all excitation range (by a variable neutral density filter). The integrated upconversion luminescence (UCL) intensity from each emitting state of $Tm^{3+}$ ions was then plotted against excitation wavelength to obtain the UCL excitation spectrum. The UCL peaked at 340 nm ($^1I_6 \rightarrow {}^3F_4$), and at 350, 450, and 510 nm (from $^1D_2$ state to $^3H_6$, $^3F_4$, and $^3H_5$ states), as well as at 480 and 650 nm (from $^1G_4$ to $^3H_6$ and $^3F_4$), are corresponding integrated to produce an integrated intensity from the $^1I_6$, $^1D_2$, and $^1G_4$ states. A tunable Ti: Sapphire laser (Tsunami from Spectra Physics) operating in free-running mode (no mode-locking) and providing quasi continuous wave (CW) excitation in the range of 750-880 nm was also used to obtain the excitation spectra, which were identical to those obtained with femtosecond pulsed excitation with Chameleon, confirming independence of UCL excitation spectra from that whether laser excitation was CW or femtosecond pulsed with high repetition rate.

***Photography and Photostability.*** Photographic images of UCL from nanoparticle solution dispersed in DMF, home-made IR card, and commercial IR card were taken by a digital camera of iPhone 5s (Apple Inc) without any optical filters. Those images were taken under laser excitation with wavelengths ranging from 700 to 1080 nm (at a 10 nm step) at a power density of ~1 W/cm$^2$. The tunable wavelengths were provided by a Ti: Sapphire laser (Chameleon from Coherent). Incoherent light upconversion was also photographed using iPhone 5s but with an optical filter (700 nm short pass). To obtain pattern to be photographed, an incandescent light of a halogen lamp (12 V-100 W) installed in an inverted Nikon microscope (Eclipse TE 2000), was directed through a hand-made mask with shapes of letters and an optical filter (750-1100 nm band pass), and then focused onto our home-made IR card, producing UCL from mask-projected letters. The power

density of the spectrally selected by filters lamp light (750-1100 nm region) on the surface of IR card was measured to be ~ 0.016 W/cm$^2$. To compare the photostability of home-made and commercial IR cards, both cards were irradiated with a power density of ~1 W/cm$^2$ at 810 nm for 5 minutes, and UCL photographs were taken at different time points. In addition, the intensities of UCL from both IR cards were recorded by the Fluorolog-3.11 Jobin Yvon spectrofluorometer at the same time points. The photostability of home-made IR card at ~980 nm (power density, ~1 W/cm$^2$) was also measured and used as a reference, which shows no photobleaching due to a straightforward excitation of $Yb^{3+}$ ions without the involvement of multistep energy transfer from NIR dyes.

## B. Synthetic Procedures

### B1. Synthesis of β-$NaYbF_4$:$Tm^{3+}$ 0.5% @$NaYF_4$:$Nd^{3+}$ x% Core/Shell Upconversion Nanoparticles

Synthesis of β-$NaYbF_4$:$Tm^{3+}$ 0.5% @$NaYF_4$:$Nd^{3+}$ x% (x=0, 3, 5, 8, 10, 15, 20, 30, 50) core/shell upconversion nanoparticles was performed using a three-step procedure developed from a recent thermolysis approach.[2] The first two steps involve the synthesis of the cubic phase core (α-$NaYbF_4$:$Tm^{3+}$ 0.5%), and its subsequent conversion to the hexagonal phase (β-$NaYbF_4$:$Tm^{3+}$ 0.5%). The yields of all the obtained nanocrystals in step1 and step 2 were 60-70%, when taking into account the ligand weight.[2] We assumed a stoichiometric production of the cubic phase core (α-$NaYbF_4$:$Tm^{3+}$ 0.5%) in the first step (1 mmol), and the hexagonal phase (β-$NaYbF_4$:$Tm^{3+}$ 0.5%) in the second step (0.5 mmol). The last step involves coating of the β-$NaYF_4$:$Nd^{3+}$ y% shell onto the hexagonal core using a seed-mediated epitaxial growth process.

***Step 1***. *Synthesis of α-$NaYbF_4$:$Tm^{3+}$ 0.5 % core*: In a typical synthesis of the cubic core, $Yb_2O_3$ (0.4975 mmol) and $Tm_2O_3$ (0.0025 mmol) was mixed with 10 mL of 50% trifluoroacetic acid in a 100 mL three-necked flask and then refluxed at 95 ℃ until completely dissolved. The clear solution will then be evaporated to dryness under argon gas purge to obtain 1.0 mmol $RE(CF_3COO)_3$ (RE=Yb+Tm) precursor. Sodium trifluoroacetate (2.0 mmol) was added together with oleic acid (8 mL, 90% tech grade), oleylamine (8 mL, 70% tech grade) and octadecene (12 mL, 90% tech grade). The solution was degassed at 120 ℃ for 30 min under argon gas to remove the remaining water and oxygen. The resulting solution will then be heated to 300 ℃ at a rate of ~15 ℃/min and kept at this temperature for 30 minutes before naturally cooling down to room temperature. 10 mL ethanol to precipitate the nanocrystals was added followed by centrifugation at 18144 rcf for 7 minutes. The collected precipitate was dispersed in 10 mL hexane without further washing to avoid loss of the cubic core product.

***Step 2.*** *Synthesis of β-$NaYbF_4$:$Tm^{3+}$ 0.5 % core*: To convert the α-$NaYbF_4$:$Tm^{3+}$ to the hexagonal phase, 5 mL of the hexane solution containing 0.5 mmol cubic core was added to a mixture of sodium trifluoroacetate (1.0 mmol), oleic acid (10 mL) and octadecene (10 mL). Residual water and oxygen was again removed by degassing at 120 ℃ for 30 min under Ar. The resulting solution will then be heated to 320 ℃ (~15 ℃/min) and kept at this temperature for 30 minutes before naturally cooling down to room temperature. Excess ethanol will then be added to precipitate the nanocrystals followed by centrifugation at 18144 rcf for 7 minutes. The collected β-$NaYbF_4$:$Tm^{3+}$(x%) crystals will then be dispersed in 5 mL hexane.

***Step 3.*** *Synthesis of β-$NaYbF_4$:$Tm^{3+}$ 0.5%@β-$NaYF_4$:$Nd^{3+}$ x% core/shell* nanoparticles: The $RE(CF_3COO)_3$ shell precursor was first prepared by mixing $Y_2O_3$ (0.25-0.25×x% mmol) and $Nd_2O_3$ (0.25×x% mmol) with 50% concentrated trifluoroacetic acid, refluxing at 95 ℃ to get a clear solution, and then evaporating the solution to dryness under argon gas in a three-neck flask. Subsequently, the β-$NaYbF_4$:$Tm^{3+}$0.5% core (0.5 mmol) in 10 mL hexane, the $Na(CF_3COO)$ (1.0 mmol), 10 mL oleic acid and 10 mL octadecene were added into the flask. The mixture was heated at 80 ℃ for 30 min to remove hexane, and then degassed at 120 ℃ for 30 min under argon gas to

remove the remaining water and oxygen. Lastly, the resulting solution were heated to 320 ℃ at a rate of ~15 ℃/min and kept at this temperature for 30 minutes before naturally cooling down to room temperature. 10 mL ethanol to precipitate the nanocrystals was added followed by centrifugation at 18144 rcf for 7 minutes.

**B2. Synthesis of β-$NaYbF_4$:$Er^{3+}$ 2% @$NaYF_4$:$Nd^{3+}$ 30% and β-$NaYbF_4$:$Ho^{3+}$ 2% @$NaYF_4$:$Nd^{3+}$ 30%Core/Shell Upconversion Nanoparticles.**

Both types of nanoparticles were prepared using a three-step procedure as described for the preparation of β-$NaYbF_4$:$Tm^{3+}$ 0.5% @$NaYF_4$:$Nd^{3+}$ 30% core/shell upconversion nanoparticles (B1 section). The difference is that the $Tm^{3+}$ precursor was replaced by the corresponding amounts of $Er^{3+}$ or $Ho^{3+}$ precursors. All other synthetic parameters were kept the same.

**Table S1.** The amounts of precursors used in preparation of β-$NaYbF_4$:$Er^{3+}$ 2% @$NaYF_4$:$Nd^{3+}$ 30% and β-$NaYbF_4$:$Ho^{3+}$ 2% @$NaYF_4$:$Nd^{3+}$ 30% core/shell samples using the three step procedure.

| | $Yb_2O_3$ mmol | $Er_2O_3$($Ho_2O_3$) mmol | $Y_2O_3$ mmol | $Nd_2O_3$ | $Na(CF_3COO)$ mmol |
|---|---|---|---|---|---|
| α-$NaYbF_4$:$Er^{3+}$2% (Ho) | 0.49 | 0.01 | 0 | 0 | 2 |
| β-$NaYbF_4$:$Er^{3+}$2% (Ho) | 0 | 0 | 0 | 0 | 2 |
| β-$NaYbF_4$:$Er^{3+}$2%(Ho)@$NaYF_4$:$Nd^{3+}$30% | 0 | 0 | 0.35 | 0.15 | 2 |

**B3. Synthesis of β-$NaYF_4$:$Yb^{3+}$ 30%, $Tm^{3+}$ 0.5% @$NaYF_4$ Core/Shell Upconversion Nanoparticles.**

These nanoparticles were also prepared using a three-step procedure as described for the preparation of β-$NaYbF_4$:$Tm^{3+}$ 0.5% @$NaYF_4$:$Nd^{3+}$ x% core/shell upconversion nanoparticles (B1 section). The difference was in that the $Yb_2O_3$ (0.4975 mmol) and $Tm_2O_3$ (0.0025 mmol) were replaced by $Y_2O_3$ (0.325 mmol), $Yb_2O_3$ (0.15 mmol), and $Tm_2O_3$ (0.0025 mmol) in the first step, and no $Nd_2O_3$ were involved in the third step to prepare the shell precursor. All other synthetic parameters were kept the same.

**Table S2.** The amounts of precursors used in preparation of β-$NaYF_4$:$Yb^{3+}$ 30%, $Tm^{3+}$ 0.5% @$NaYF_4$ core/shell samples using the three step procedure.

| | $Yb_2O_3$ mmol | $Tm_2O_3$ mmol | $Y_2O_3$ mmol | $Na(CF_3COO)$ mmol |
|---|---|---|---|---|
| α-$NaYbF_4$:$Tm^{3+}$0.5% | 0.4975 | 0.0025 | 0 | 2 |
| β-$NaYbF_4$: $Tm^{3+}$0.5% | 0 | 0 | 0 | 2 |
| β-$NaYbF_4$: $Tm^{3+}$0.5%@$NaYF_4$ | 0 | 0 | 0.5 | 2 |

**B4. Synthesis of β-$NaYF_4$:$Yb^{3+}$ 30% @$NaYF_4$:$Nd^{3+}$ 3% and β-$NaYbF_4$@$NaYF_4$:$Nd^{3+}$ 3%,**

**Core/Shell Nanoparticles.**

These nanoparticles were prepared using a three-step procedure as described for the preparation of β-$NaYbF_4$:$Tm^{3+}$ 0.5% @$NaYF_4$:$Nd^{3+}$ x% core/shell upconversion nanoparticles (B1 section). The difference lies in that the molar ratio between the Yb precursor and the Y precursor for the cubic phase core preparation (step 1) as well as the molar ratio between the Nd precursor and the Y precursor for the hexagonal phase (step 3) were adjusted accordingly here. No $Tm^{3+}$ ions were involved here. All other synthetic parameters were kept the same.

**B5. Synthesis of β-$NaYF_4$:$Nd^{3+}$ 5% Downconversion Nanoparticles.**

The synthesis of β-$NaYF_4$:$Nd^{3+}$ 5% nanoparticles was adapted from our recent work by growing the nuclei at low temperature via ion diffusion, with subsequent Ostwald-Ripening at higher temperature.[3] The combined amount of $YCl_3$•$6H_2O$ (0.95 mmol) and $NdCl_3$•$6H_2O$ (0.05 mmol) were dissolved in 1 mL distilled $H_2O$ in a 100 mL three-necked flask prior to addition of 6 mL oleic acid (90%, technical grade) and 10 mL 1-octadecene (70%, technical grade). The mixture was heated to 160 °C and maintained for 1 h under Ar gas with constant stirring to remove $H_2O$ and $O_2$. The solution was then cooled to 50 °C, before slowly adding 10 mL solution of methanol containing 4 mmol $NH_4F$ and 2.5 mmol NaOH. After stirring for 30 minutes, methanol was evaporated at 80 °C for 30 minutes. The temperature was subsequently increased to 300 °C at a rate of ~15 °C/min and maintained for 1.5 h under Ar gas protection. The final solution was cooled to room temperature; the resulting nanoparticles were collected by adding an excess amount of acetone and then centrifuged at 27104 rcf for 10 minutes. The precipitate was washed with a 1:1 mixture of ethanol/$H_2O$ and finally dispersed in 10 mL hexane for further uses.

**B6. Synthesis of β-($NaYF_4$:$Yb^{3+}$ 20%, $Tm^{3+}$ 0.5%, $Nd^{3+}$1%)@$NaYF_4$:$Nd^{3+}$20% Upconversion Nanoparticles.**

These UC nanoparticles, used as a reference for UCL comparison, were prepared following exactly the procedure reported recently.[4]

**B7. Synthesis of IR-808 dye.**

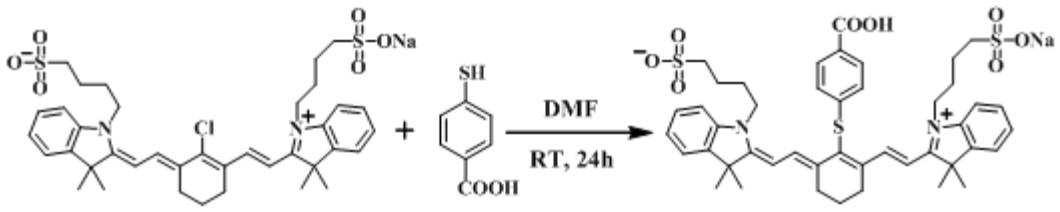


**Scheme S1.** Synthesis of IR-808 dye.

The functionalization reaction was performed via a standard Schlenk-line technique in dry glassware and under a dry $N_2$ atmosphere using an adapted procedure from a literature.[5] A solution of IR-783 (100 mg, 0.12 mmol) and 4-mercaptobenzoic acid (80 mg, 0.24 mmol) in DMF (5 mL)

was mixed at room temperature for 24 hours. Then, diethyl ether (50 mL) was added slowly to precipitate the product. After the solution was filtered through a 0.45 μm PTFE syringe, the precipitate was collected by centrifugation, washed with diethyl ether, and then vacuum dried to yield 80 mg (0.1 mmol, 82%) of IR-808 crystals. $^{1}$H NMR (400MHz, d$^{6}$-DMSO): 8.51(d, 2H, J=14), 7.84(d, 2H, J=8.4), 7.51(d, 2H, J=7.2), 7.42(d, 2H, J=8), 7.36(d, 2H, J=8.4), 7.36(t, 2H, J=8), 7.20(t, 2H, J=7.2), 6.39(d, 2H, J=14), 4.16(t, 4H, J=6.8), 2.78(t, 4H, J=6), 1.93(t, 2H, J=5.2),1.74(m, 10H), 1.36(s, 12H). MS: calculated for $C_{45}H_{51}O_8S_3N_2$: 843.2808; found: 843.3586.

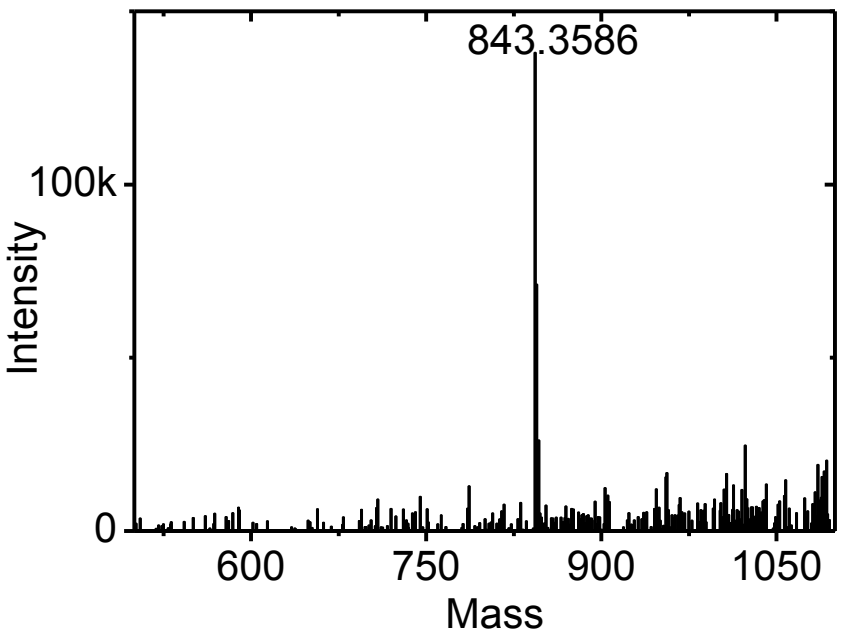


**Figure S1.** HRMS spectrum of IR-808.

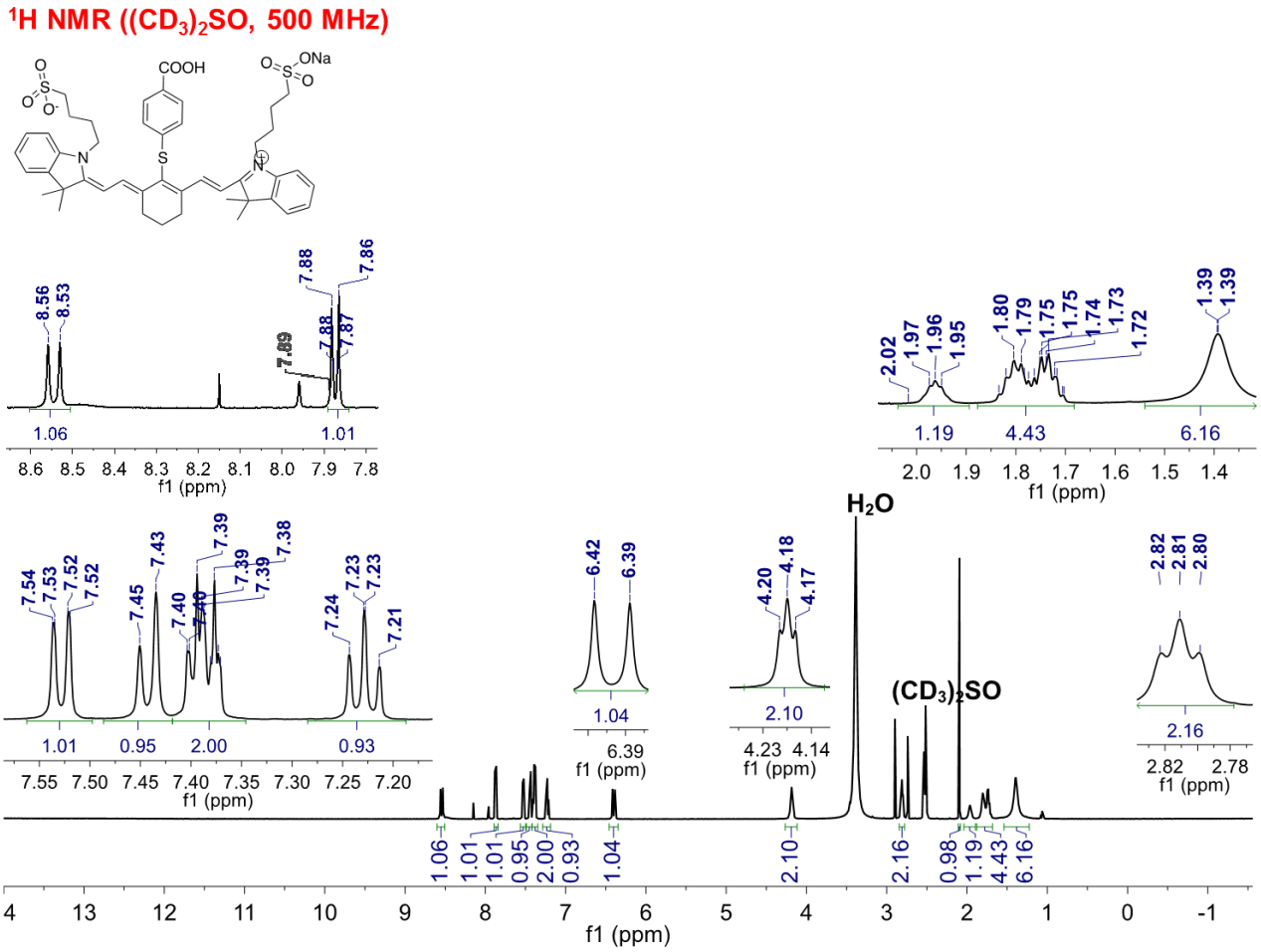


**Figure S2.** $^{1}$H-NMR (500 MHz, $(CD_3)_2SO$) spectrum of IR-808.

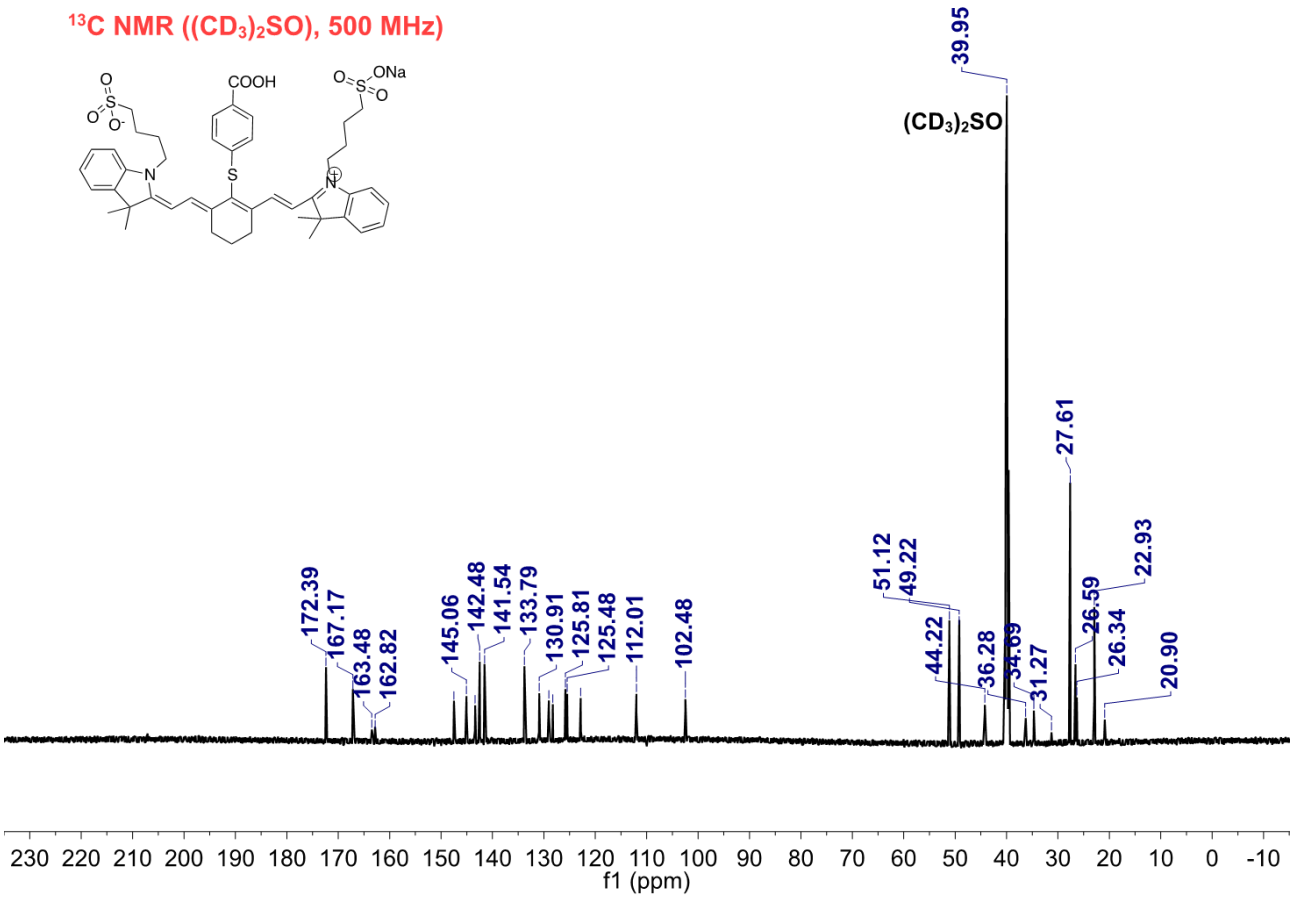


**Figure S3.** $^{13}$C-NMR (500 MHz, $(CD_3)_2SO$) spectrum of IR-808.

## C. Sample Preparations

### C1. NIR Dye-Sensitized Lanthanide-Doped Nanoparticles in DMF.

Here lanthanide-doped nanoparticles refer to all types of inorganic nanoparticles involved in NIR dye-sensitization experiments. These inorganic nanoparticles include β-$NaYF_4$:$Nd^{3+}$ 5% downconversion nanoparticles, β-$NaYbF_4$: $Tm^{3+}$ 0.5% upconversion nanoparticles, β-($NaYbF_4$: $Tm^{3+}$ 0.5%)@ $NaYF_4$: $Nd^{3+}$ x% (x=0, 6, 10, 20, 30, 50) core/shell upconversion nanoparticles, β-($NaYbF_4$: $Tm^{3+}$ 0.5%)@ $NaLuF_4$: $Nd^{3+}$ 30% core/shell upconversion nanoparticles, β-($NaYbF_4$: $Er^{3+}$ 2%)@ $NaYF_4$: $Nd^{3+}$ 30% core/shell upconversion nanoparticles, and β-($NaYbF_4$: $Ho^{3+}$ 2%)@ $NaYF_4$: $Nd^{3+}$ 30% core/shell upconversion nanoparticles. The involved NIR dyes include IR-808, IR-806 and IR-820. All IR dye sensitized experiments in solution used the same procedure as follows.

***Preparation of $NOBF_4$ coated lanthanide-doped nanoparticles.*** The oleic acid ligands on the surface of these lanthanide-doped nanoparticles were first replaced with sub-nanometer ligands of nitrosonium tetrafluoroborate ($NOBF_4$) using an adapted procedure from literature.[6] During this ligand exchange process, 5 mL of oleic acid coated nanoparticles dispersed in hexane (~10 mg/mL) was mixed with a 5 mL N,N-dimethylformamide (DMF) solution of $NOBF_4$ (0.01 M) at room temperature. The resulting mixture was shaken gently for 10 minutes, allowing an extraction of nanoparticles from upper hexane layer into the bottom DMF layer. After disposing the hexane layer, these nanoparticles dispersed in the DMF were purified by adding a large amount of toluene and hexane (1:1 v/v) and centrifugation at 11000 rpm for 15 minutes. Subsequently, the precipitated nanoparticles were weighted and re-dispersed in DMF (for NIR dye-sensitized experiments in solution) or chloroform (for security and IR card sample preparation). A nanoparticle concentration of ~8.3 mg/mL was utilized for NIR dye sensitization experiment. All nanoparticle solutions were stored at room temperature.

***Preparation of IR dye solution in DMF.*** The involved NIR dyes were weighed and dissolved in DMF to produce a concentration of 1 mg/mL. After that, the bottled dye solution was purged with gentle argon gas flow and sealed with a parafilm. The dye solution was then covered with aluminum foil and stored in darkness to avoid light induced degradation, if any.

***Preparation of IR dye-sensitized nanoparticles solution in DMF.*** The 1 mL lanthanide-doped nanoparticle solution dispersed in DMF (~8.3 mg/mL) was mixed with an appropriate amount of dye (or dye combination) solution (1 mg/mL) to produce a defined amount NIR dye concentration in the mixture.

### C2. Preparation of Samples for Security, IR Card, and Incoherent Light Upconversion.

***Sample for Proof of Concept Security Application.*** About 20 mg polystyrene beads was added into 1 mL IR-808-Sensitized β-($NaYbF_4$: $Tm^{3+}$ 0.5%)@ $NaYF_4$: $Nd^{3+}$ 30% core/shell nanoparticles dispersed in chloroform (4 mg/mL) to prepare a semitransparent viscous mixture. This viscous mixture was then cast through a home-made letter mask to print the letter pattern on a clean microscope slide. This microscope glass slide was cleaned via sonication in acetone for 10 minutes

and then dried in air. The evaporation of chloroform produces stable upconverting pattern of letters consisting of polymer and UC nanoparticles.

***Sample for IR Card.*** IR-820 and IR-806 co-sensitized β-($NaYbF_4$: $Tm^{3+}$ 0.5%)@ $NaYF_4$: $Nd^{3+}$ 30% core/shell nanoparticles were embedded in a thick polystyrene film to form the home-made IR card. The IR-820 and IR-806 co-sensitized β-($NaYbF_4$: $Tm^{3+}$ 0.5%)@ $NaYF_4$: $Nd^{3+}$ 30% core/shell nanoparticle solution (41.5 mg) were first prepared via mixing 41.5 mg $NOBF_4$ coated core/shell nanoparticles and 0.15 mg total of IR-820 and IR-806 (1:1) in 1 mL $CHCl_3$ solvent. Then, 0.1 g of polystyrene beads (MW 280,000) was added into this solution, which was then sonicated for 5 minutes to dissolve the polystyrene beads and to produce a homogeneous viscous solution. The resulting solution is then casted onto a glass slide and air dried until all the solvent evaporated.

***Sample for Incoherent Light Upconversion.*** The sample of home-made IR card was also utilized for demonstration of incoherent light upconversion without any modifications.

## D. Supporting Figures for Core/Shell Nanostructures

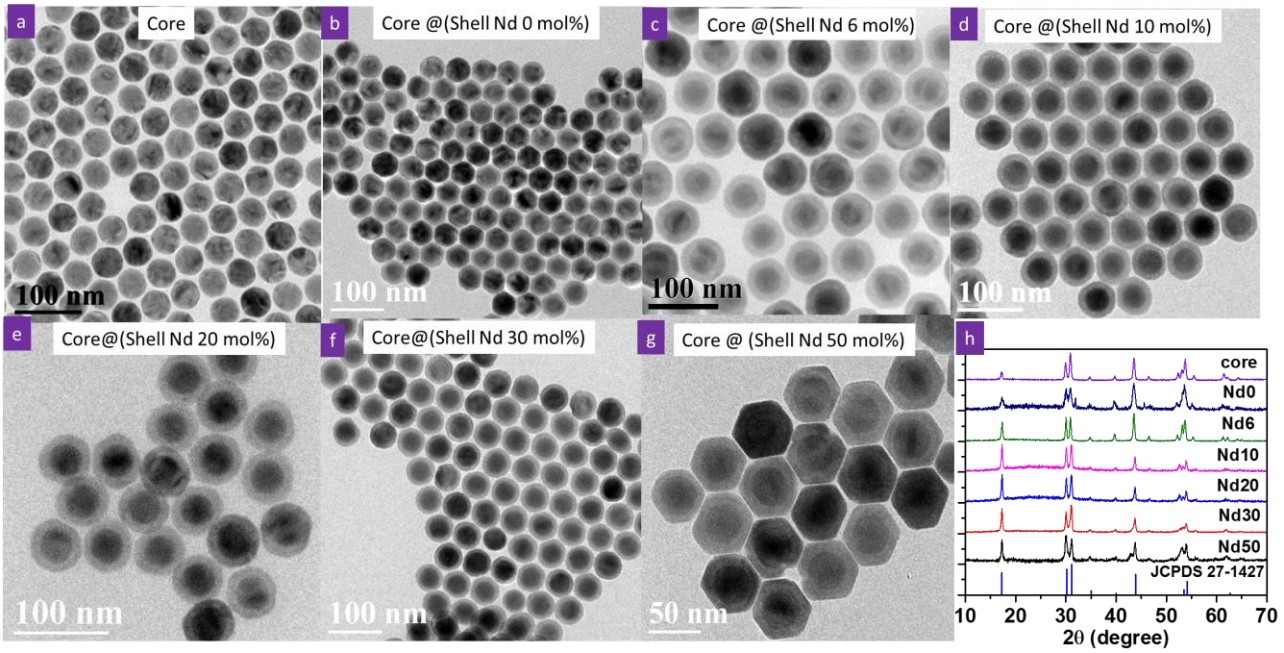


**Figure S4.** Transmission electron microscopic (TEM) images and x-ray diffraction (XRD) patterns of the core and core/shell nanostructures. TEM images of nanoparticles of (**a**) β-$NaYbF_4$: $Tm^{3+}$ 0.5% core, (**b**) β-($NaYbF_4$: $Tm^{3+}$ 0.5%)@ $NaYF_4$ core/shell, (**c**) β-($NaYbF_4$: $Tm^{3+}$ 0.5%)@ $NaYF_4$: $Nd^{3+}$ 6% core/shell, (**d**) β-($NaYbF_4$: $Tm^{3+}$ 0.5%)@ $NaYF_4$: $Nd^{3+}$ 10% core/shell, (**e**) β-($NaYbF_4$: $Tm^{3+}$ 0.5%)@ $NaYF_4$: $Nd^{3+}$ 20% core/shell, (**f**) β-($NaYbF_4$: $Tm^{3+}$ 0.5%)@ $NaYF_4$: $Nd^{3+}$ 30% core/shell, (**e**) β-($NaYbF_4$: $Tm^{3+}$ 0.5%)@ $NaYF_4$: $Nd^{3+}$ 50% core/shell structure. (**h**) The XRD patterns for the samples shown in (**a-g**). The standard pattern JCPDS 27-1427 of hexagonal phase $NaYbF_4$ host material is included as a reference. These results confirm the formation of epitaxial hexagonal phase β-($NaYbF_4$: $Tm^{3+}$ 0.5%)@ $NaYF_4$: $Nd^{3+}$ x% (x=0, 6, 10, 20, 30, 50) core/shell nanostructures.

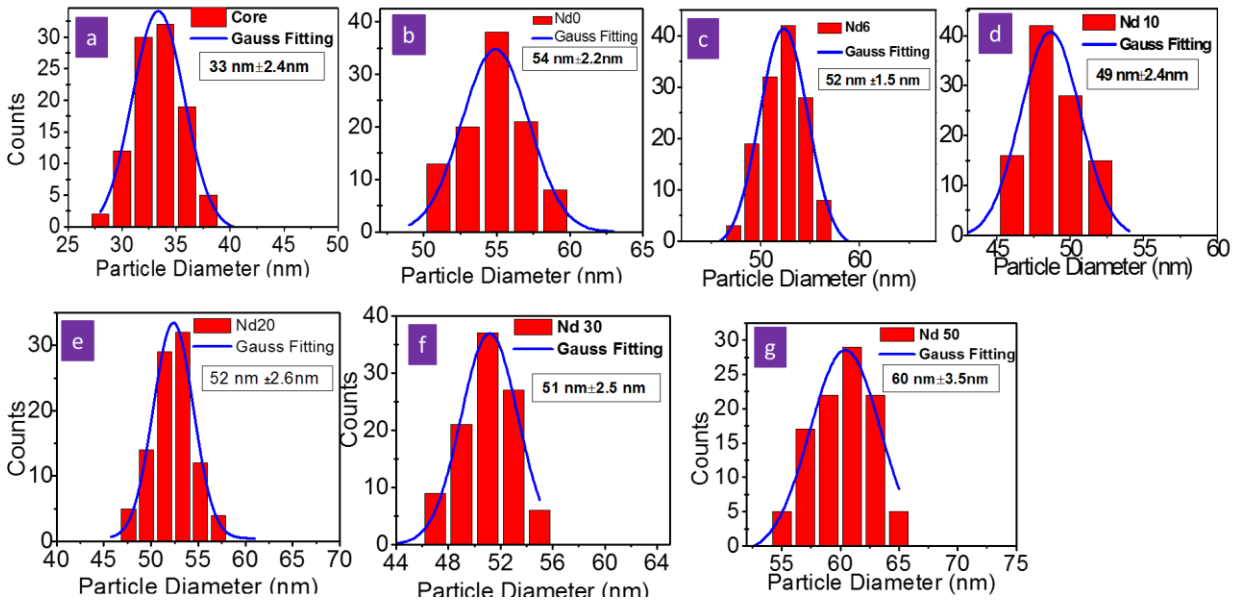


**Figure S5.** Histograms of the size distribution for the (**a**) β-$NaYbF_4$: $Tm^{3+}$ 0.5% core, (**b**) β-($NaYbF_4$: $Tm^{3+}$ 0.5%)@ $NaYF_4$ core/shell, (**c**) β-($NaYbF_4$: $Tm^{3+}$ 0.5%)@ $NaYF_4$: $Nd^{3+}$ 6% core/shell, (**d**) β-($NaYbF_4$: $Tm^{3+}$ 0.5%)@ $NaYF_4$: $Nd^{3+}$ 10% core/shell, (**e**) β-($NaYbF_4$: $Tm^{3+}$ 0.5%)@ $NaYF_4$: $Nd^{3+}$ 20% core/shell, (**f**) β-($NaYbF_4$: $Tm^{3+}$ 0.5%)@ $NaYF_4$: $Nd^{3+}$ 30% core/shell, (**g**) β-($NaYbF_4$: $Tm^{3+}$ 0.5%)@ $NaYF_4$: $Nd^{3+}$ 50% core/shell nanoparticles.

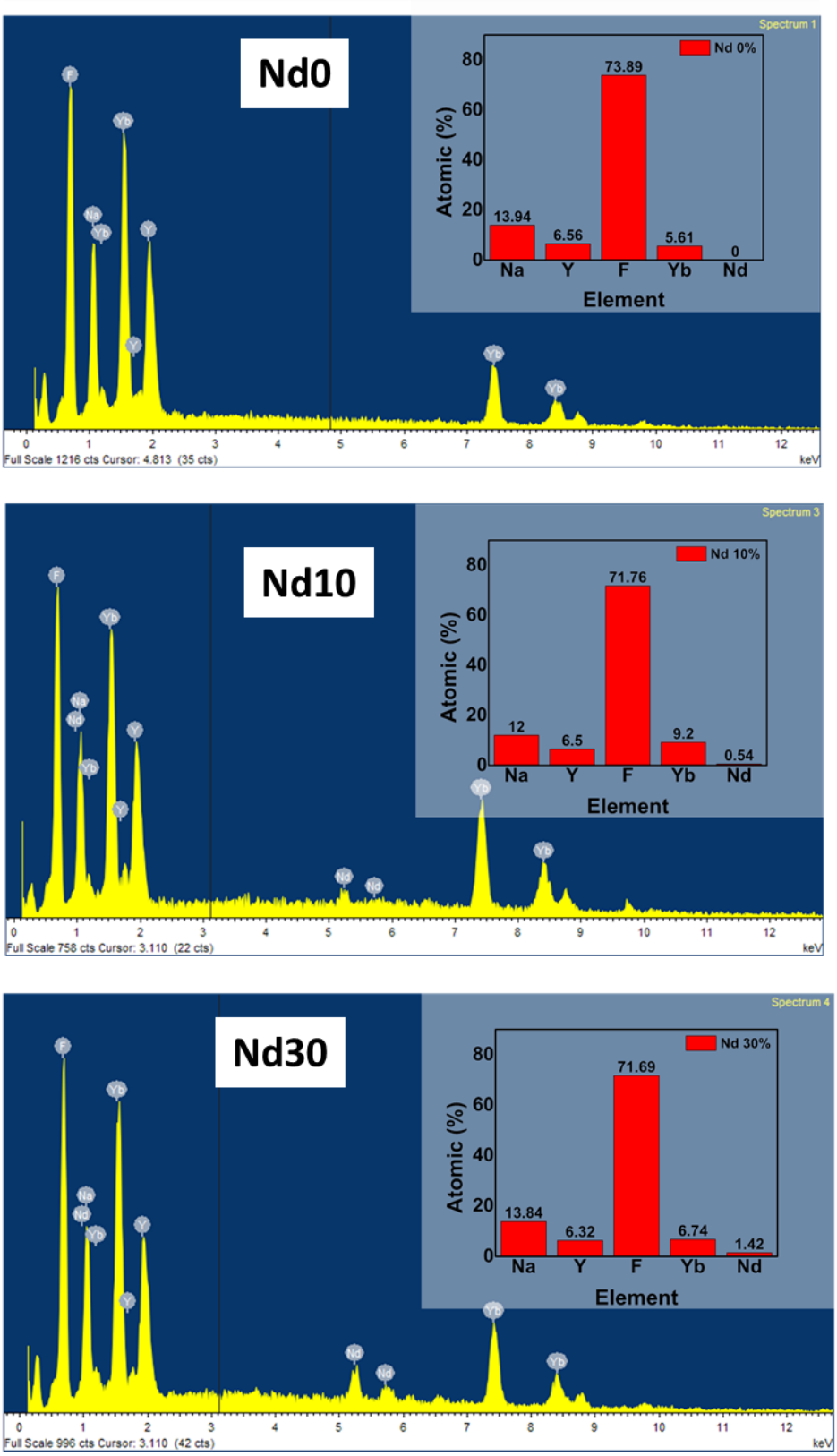


**Figure S6.** The energy-dispersive X-ray spectroscopy (EDX) of the exemplified samples of β-($NaYbF_4$: $Tm^{3+}$ 0.5%)@$NaYF_4$, β-($NaYbF_4$: $Tm^{3+}$ 0.5%)@ $NaYF_4$: $Nd^{3+}$ 10% core/shell, and β-($NaYbF_4$: $Tm^{3+}$ 0.5%)@ $NaYF_4$: $Nd^{3+}$ 30% core/shell nanoparticles. A gradual increase of peak intensities for $Nd^{3+}$ element is observed, in agreement with intended increase of $Nd^{3+}$ dopants in the shell during the synthesis.

**Table S3.** Inductively coupled plasma mass spectrometric (ICP-MS) results of β-($NaYbF_4$: $Tm^{3+}$ 0.5%)@$NaYF_4$ core/shell, β-($NaYbF_4$: $Tm^{3+}$ 0.5%)@ $NaYF_4$: $Nd^{3+}$ 10% core/shell, β-($NaYbF_4$: $Tm^{3+}$ 0.5%)@ $NaYF_4$: $Nd^{3+}$ 20% core/shell, and β-($NaYbF_4$: $Tm^{3+}$ 0.5%)@ $NaYF_4$: $Nd^{3+}$ 30% core/shell nanoparticles. These results indicate a stoichiometric synthesis of $Nd^{3+}$-sensitized hexagonal fluoride core/shell nanocrystals.

| Nd series | 89Y (ppb) | 146Nd (ppb) | 169Tm (ppb) | 173Yb (ppb) | Y (µM) | Nd (µM) | Tm (µM) | Yb (µM) |
|---|---|---|---|---|---|---|---|---|
| **0** | 77.9106 | 0 | 1.88773 | 261.749 | 0.8754 | 0 | 0.01117 | 1.513 |
| **10** | 70.3011 | 12.37788 | 1.04273 | 249.985 | 0.7899 | 0.08478 | 0.00617 | 1.445 |
| **20** | 4.88165 | 2.23526 | 0.12675 | 20.1199 | 0.05485 | 0.01531 | 0.00075 | 0.1163 |
| **30** | 20.9862 | 14.38392 | 0.38363 | 131.8087 | 0.2358 | 0.09852 | 0.00227 | 0.7619 |

| Nd series | % in shell | | % in core | | % Element in the core-shell structure | | | |
|---|---|---|---|---|---|---|---|---|
| | Y | Nd | Tm | Yb | Y | Nd | Tm | Yb |
| **0** | 100 | 0 | 0.73 | 99.27 | 36.48 | 0 | 0.47 | 63.05 |
| **10** | 90.31 | 9.69 | 0.43 | 99.57 | 33.96 | 3.65 | 0.27 | 62.13 |
| **20** | 78.18 | 21.82 | 0.64 | 99.36 | 29.30 | 8.18 | 0.40 | 62.12 |
| **30** | 70.53 | 29.47 | 0.30 | 99.70 | 21.47 | 8.97 | 0.21 | 69.36 |

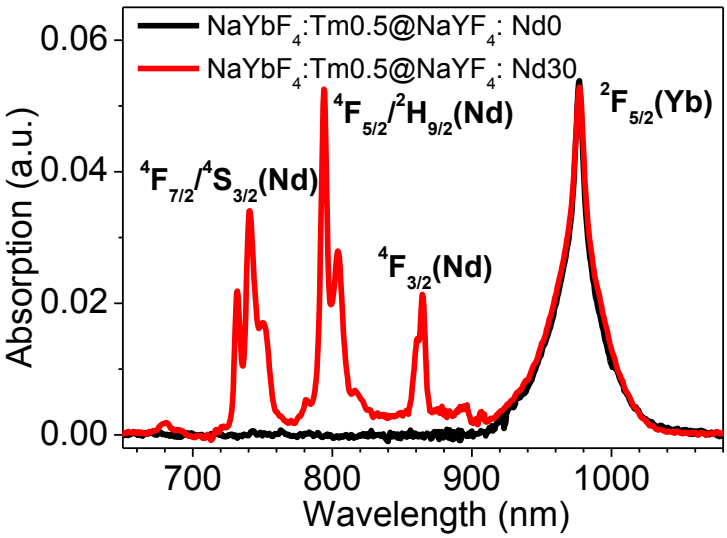


**Figure S7**. Contrasted absorption spectra of the ($NaYbF_4$: $Tm^{3+}$ 0.5%)@$NaYF_4$ (black line) and the ($NaYbF_4$: $Tm^{3+}$ 0.5%)@$NaYF_4$: $Nd^{3+}$ 30% (red line) core/shell nanoparticles (hexane dispersion).

The absorption peaks at 740, 800, and 860 nm correspond to the ground state absorption to the $^4S_{3/2}/^4S_{7/2}$, the $^4F_{5/2}/^2H_{9/2}$, and the $^4F_{3/2}$ states of $Nd^{3+}$ ions, respectively, while the absorption peak at ~ 980 nm corresponds to the $^2F_{7/2} \rightarrow {}^2F_{5/2}$ transition of $Yb^{3+}$ ions.

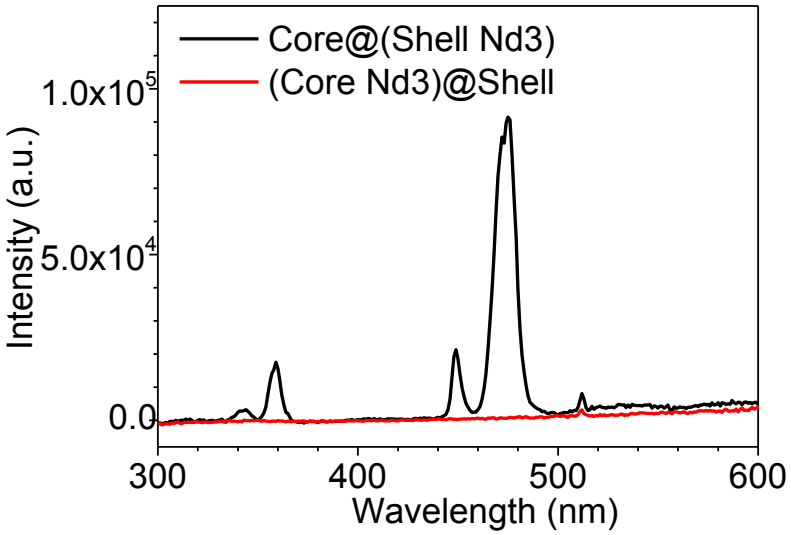


**Figure S8.** A comparison of UCL from ($NaYbF_4$: $Tm^{3+}$ 0.5%, $Nd^{3+}$ 3%)@$NaYF_4$ and ($NaYbF_4$: $Tm^{3+}$ 0.5%)@$NaYF_4$:$Nd^{3+}$ 3% core/shell nanoparticles. The significantly higher UCL intensity from the ($NaYbF_4$: $Tm^{3+}$ 0.5%)@$NaYF_4$:$Nd^{3+}$3% core/shell nanoparticle than that of the ($NaYbF_4$: $Tm^{3+}$ 0.5%, $Nd^{3+}$ 3%)@$NaYF_4$ nanoparticles manifests the importance of a spatial isolation of $Nd^{3+}$ ions from $Yb^{3+}/Tm^{3+}$ ion pairs.

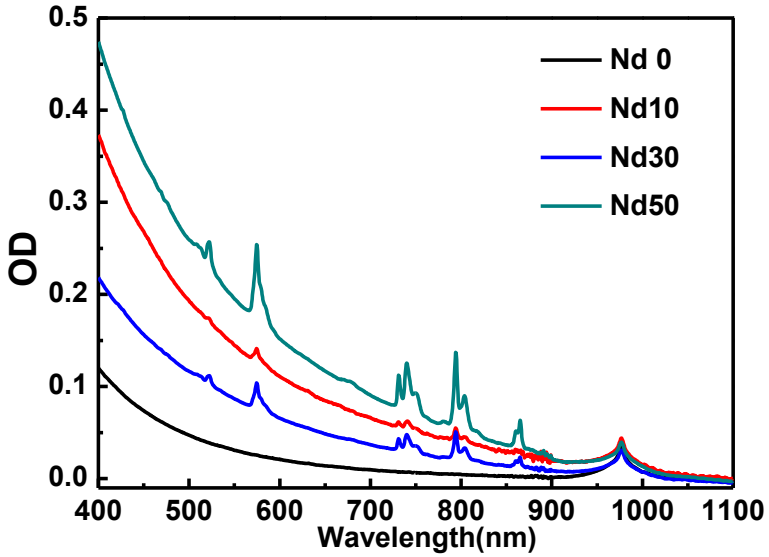


**Figure S9.** Matched absorption of β-($NaYbF_4$: $Tm^{3+}$ 0.5%)@ $NaYF_4$: $Nd^{3+}$ x% (x=0, 10, 30, 50) core/shell nanoparticles. The matching was performed at the absorption wavelength of $Yb^{3+}$ ion at ~980 nm via adjusting nanoparticle concentration of corresponding sample, ensuring each sample has an identical nanoparticle concentration. As the scattering in the NIR range at 980 nm was low, the background correction was not performed in this figure.

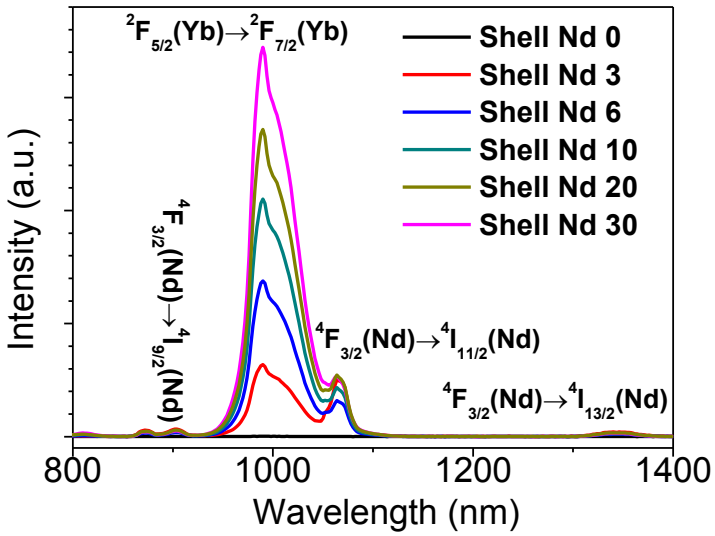


**Figure S10.** Downconversion luminescence from $Yb^{3+}$ and $Nd^{3+}$ ions in the colloidal ($NaYbF_4$: $Tm^{3+}$ 0.5%)@$NaYF_4$: $Nd^{3+}$ x% (x=0, 3, 6, 10, 20, 30) core/shell nanoparticles (hexane dispersion). Excitation at 800 nm, 10 W/cm$^2$.

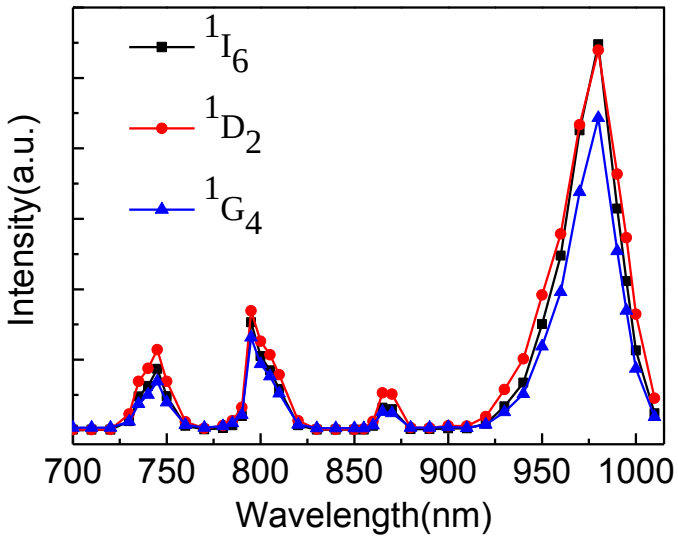


**Figure S11.** The UCL excitation spectra for the $^1I_6$, $^1D_2$, $^1G_4$ states of $Tm^{3+}$ ions in the $NaYbF_4:Tm^{3+}@NaYF_4:Nd^{3+}$ 30% core/shell nanostructure. Excitation power density of ~ 1 W/cm$^2$. The excitation spectra peaks at ~ 740, 800, and 860 nm match the absorption peaks of $Nd^{3+}$ ions in Figure S4.

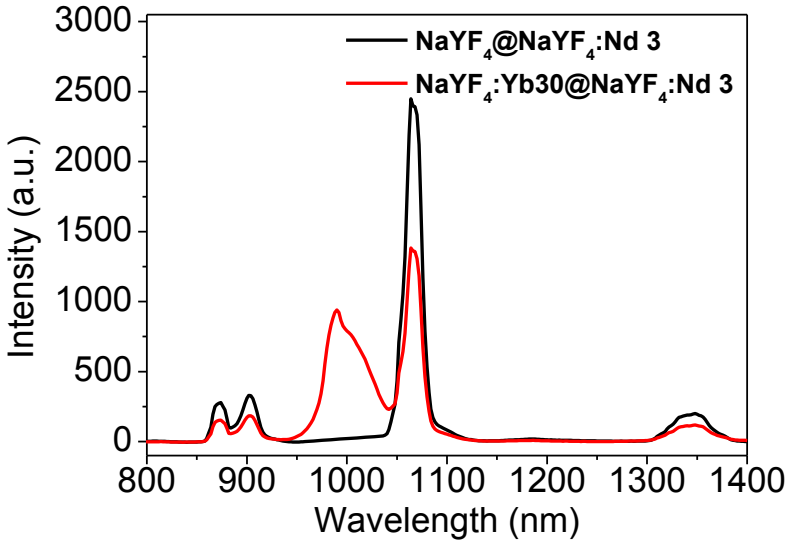


**Figure S12.** A comparison of downconversion luminescence (DCL) from the $NaYF_4@NaYF_4:Nd^{3+}$3% core/shell nanoparticles and the $NaYF_4:Yb^{3+}$ 30% $@NaYF_4:Nd^{3+}$ 3% core/shell nanoparticles (hexane dispersion, excited at ~ 800 nm). Luminescence peaks at ~860-900,

~1050, and ~1330 nm correspond to the transitions from the $^4F_{3/2}$ state to the $^4I_J$ (J=9/2, 11/2, 13/2) state of $Nd^{3+}$ ions, respectively, while the luminescence peak at ~ 980 nm corresponds to the $^2F_{5/2} \rightarrow {}^2F_{5/2}$ transition of $Yb^{3+}$ ion. In comparison with that of the $NaYF_4$@$NaYF_4$:$Nd^{3+}$3% core/shell nanoparticles, a simultaneous decrease of luminescence (at ~860-900, ~1050, and ~1330 nm) from $Nd^{3+}$ ion and appearance of luminescence from $Yb^{3+}$ ion (at ~ 980 nm) were observed for the $NaYF_4$:$Yb^{3+}$ 30% @$NaYF_4$:$Nd^{3+}$ 3% core/shell nanoparticles. This simultaneous change verifies a direct energy transfer from the $Nd^{3+}$ in the shell to the $Yb^{3+}$ in the core in the $NaYF_4$:$Yb^{3+}$ 30% @$NaYF_4$:$Nd^{3+}$ 3% core/shell nanostructure.

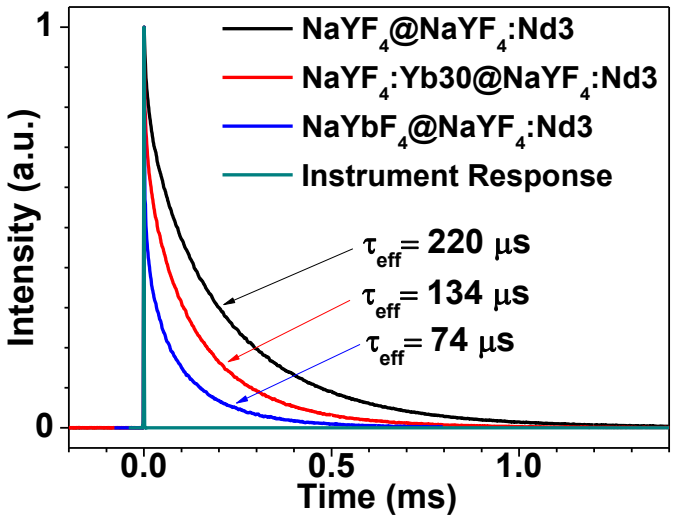


**Figure S13.** Decays of luminescence at ~860 nm (corresponding to the $^4F_{3/2} \rightarrow {}^4I_{9/2}$ transition in the $Nd^{3+}$ ions) for ($NaYF_4$:$Yb^{3+}$ x%)@$NaYF_4$: $Nd^{3+}$ 3% (x=0, 30, 100) core/shell nanoparticles. Excitation at 532 nm. The effective decay times was determined to be about 220, 134, and 74 μs for the ($NaYF_4$:$Yb^{3+}$ x%)@$NaYF_4$: $Nd^{3+}$ 3% (x=0, 30, 100) core/shell nanoparticles, respectively. This corresponds to an energy transfer efficiency of ~39% and ~66% for ($NaYF_4$:$Yb^{3+}$)@$NaYF_4$:$Nd^{3+}$3% UCNPs containing 30% and 100% $Yb^{3+}$ ions in the core, respectively.

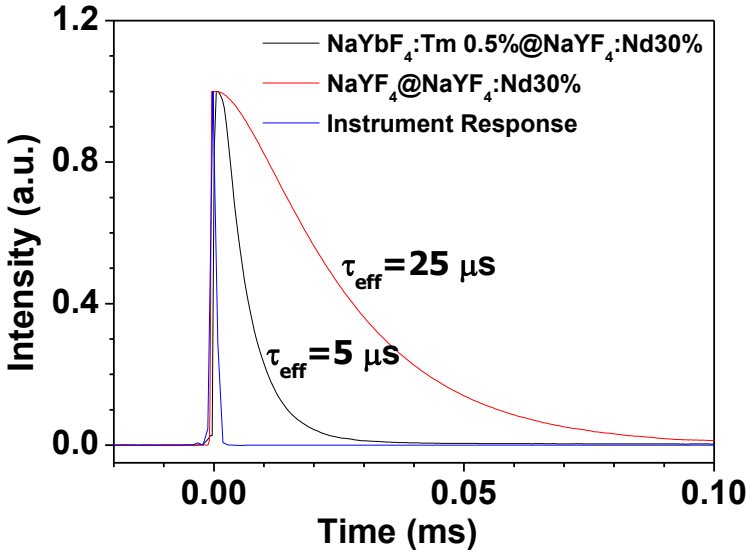


**Figure S14.** Luminescence decays of $Nd^{3+}$ ions at 860 nm ($^4F_{3/2} \rightarrow {}^4I_{9/2}$) for the $NaYbF_4:Tm^{3+}0.5\%@NaYF_4:Nd^{3+}$ 30% and the $NaYF_4@NaYF_4:Nd^{3+}$ 30% core/shell samples of similar sizes. According to equation 1 and measured lifetimes, the energy transfer efficiency from $Nd^{3+}$ to $Yb^{3+}$ ions was determined to be ~80% for the $NaYbF_4:Tm^{3+}0.5\%@NaYF_4:Nd^{3+}$ 30% core/shell structure.

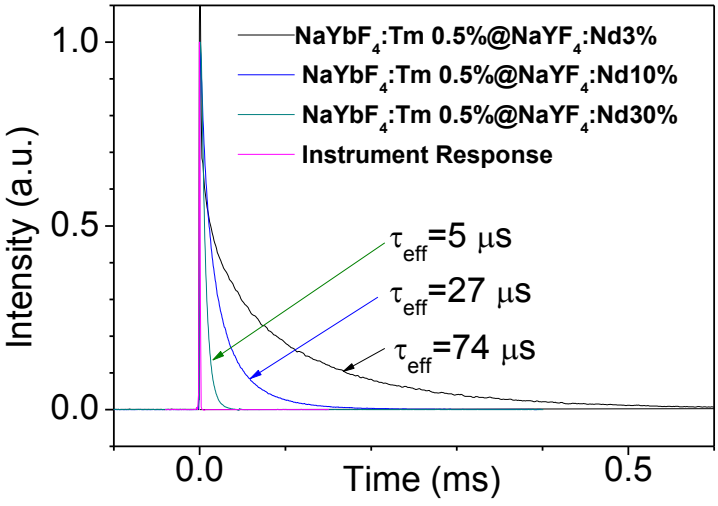


**Figure S15.** Luminescence decays of $Nd^{3+}$ ions at 860 nm ($^4F_{3/2} \rightarrow {}^4I_{9/2}$) for the $NaYbF_4:Tm^{3+}0.5\%@NaYF_4:Nd^{3+}$ x% (x=3, 10, 30) core/shell nanoparticles. An increase of $Nd^{3+}$ ions in the shell results in a significant decrease of the decay time, illustrating the elevated cross relaxation process $^4F_{3/2} + {}^4I_{9/2} \rightarrow 2{}^4I_{15/2}$ between two $Nd^{3+}$ ions.[3] This cross relaxation process

nonradiatively depopulates the excited energy of the $^4F_{3/2}$ state of $Nd^{3+}$ ions, thus limiting the amount of energy transfer from $Nd^{3+}$ to $Yb^{3+}$ to evoke multiphoton UCL.

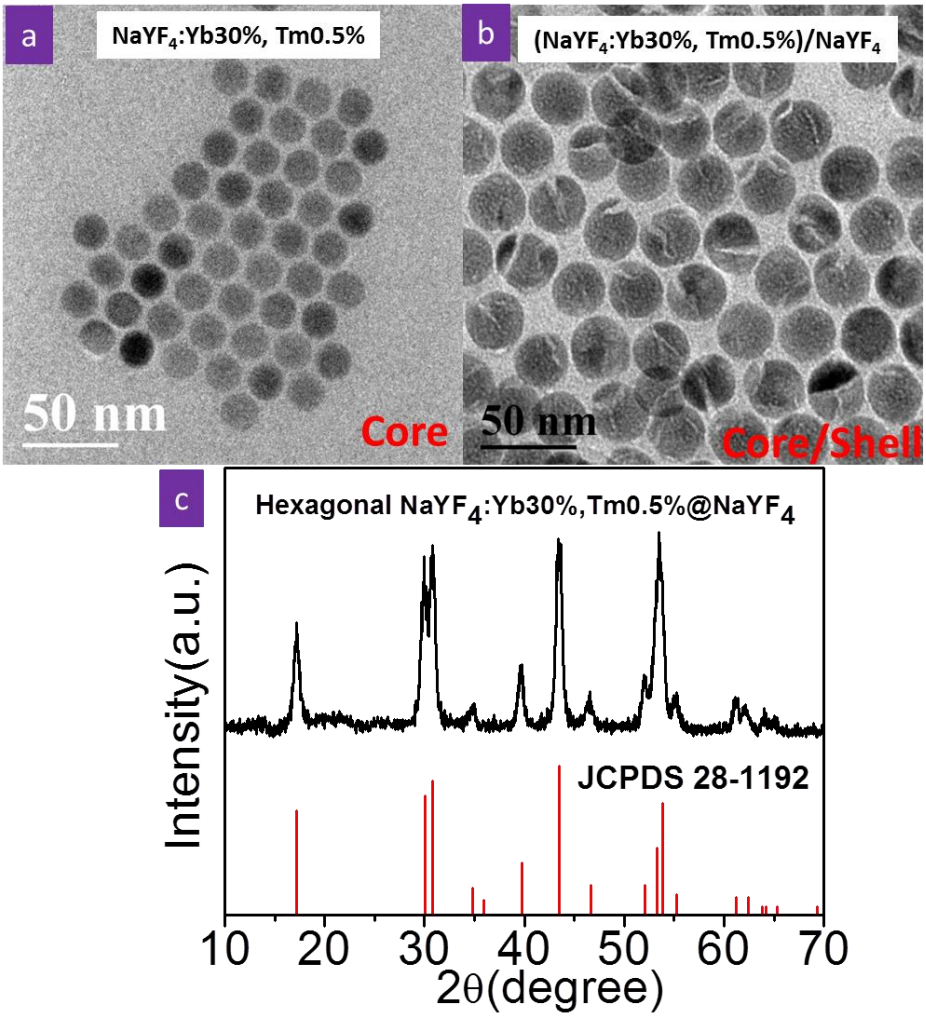


**Figure S16.** Size and phase characterizations of β-($NaYF_4$: $Yb^{3+}$ 30%, $Tm^{3+}$ 0.5%)@$NaYF_4$ core/shell nanoparticles. TEM micrographic images of (**a**) β-($NaYF_4$: $Yb^{3+}$ 30%, $Tm^{3+}$ 0.5% core nanoparticles and (**b**) β-($NaYF_4$: $Yb^{3+}$ 30%, $Tm^{3+}$ 0.5%)@$NaYF_4$ core/shell nanoparticles. (**c**) The XRD pattern of the β-($NaYF_4$: $Yb^{3+}$ 30%, $Tm^{3+}$ 0.5%)@$NaYF_4$ core/shell nanoparticles, along with the standard pattern (JCPDS 28-1192) of hexagonal phase $NaYF_4$ host lattice as a reference. The TEM and XRD results indicate the resulting β-($NaYF_4$: $Yb^{3+}$ 30%, $Tm^{3+}$ 0.5%)@$NaYF_4$ core/shell nanoparticles have an average size of ~ 30 nm and have the hexagonal crystal phase.

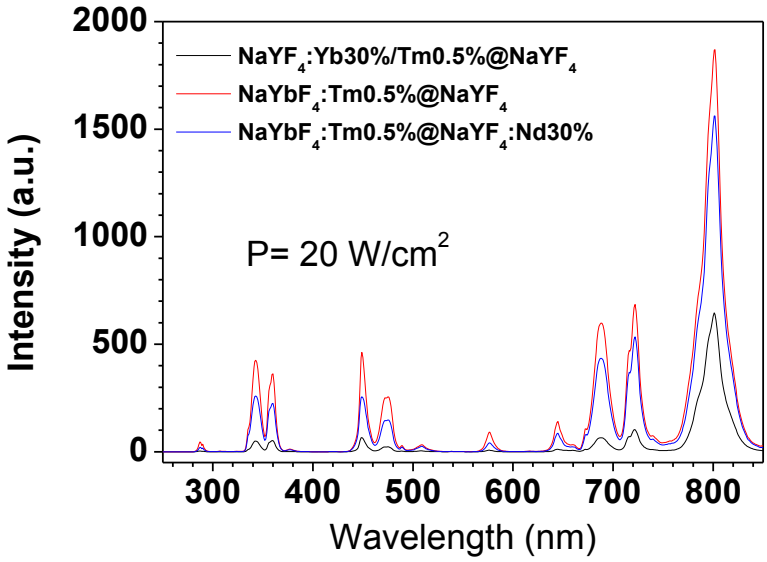


**Figure S17.** A comparison of multiphoton UCL from the optimized ($NaYbF_4$: $Tm^{3+}$ 0.5%)@$NaYF_4$: $Nd^{3+}$ 30%, the ($NaYbF_4$: $Tm^{3+}$ 0.5%)@$NaYF_4$, as well as the canonical ~ 30 nm sized $NaYF_4$:$Yb^{3+}$ 30%, $Tm^{3+}$ 0.5% @$NaYF_4$ core/shell nanoparticles under excitation at ~ 980 nm of 20 W/cm$^2$. During the comparison, the same nanoparticle concentration for each sample was utilized. UCL comparison between the ($NaYbF_4$: $Tm^{3+}$ 0.5%)@$NaYF_4$: $Nd^{3+}$ 30% and the ($NaYbF_4$: $Tm^{3+}$ 0.5%)@$NaYF_4$ sample reveals that the existence of high $Nd^{3+}$ ions in the shell has negligible effect on decreasing the UCL intensity. The integrated intensities from the upconverting luminescence of the optimized ($NaYbF_4$: $Tm^{3+}$ 0.5%)@$NaYF_4$: $Nd^{3+}$ 30% core/shell nanoparticles are six times higher than from the canonical ~ 30 nm sized $NaYF_4$:$Yb^{3+}$30%, $Tm^{3+}$0.5% @$NaYF_4$ core/shell nanoparticles (upconversion quantum yield of ~ 3.5%),[7] illustrating the highly efficient upconversion nature of the optimized core/shell sample.

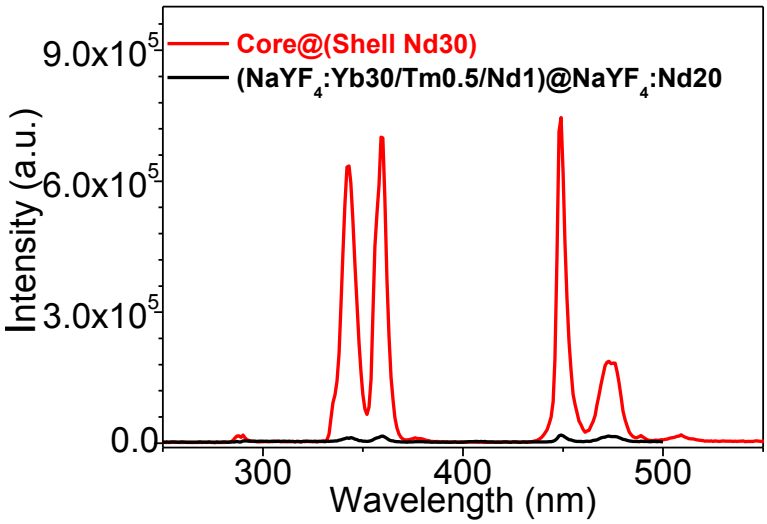


**Figure S18.** A comparison of multiphoton UCL from the optimized ($NaYbF_4$: $Tm^{3+}$ 0.5%)@$NaYF_4$: $Nd^{3+}$ 30% core/shell nanoparticles and ($NaYF_4$:$Yb^{3+}$ 20%, $Tm^{3+}$ 0.5%, $Nd^{3+}$ 1%)@$NaYF_4$:$Nd^{3+}$ 20% core/shell nanoparticles (which were previously reported to produce highly efficient UCL under 800 nm) under excitation at 800 nm of 10 W/$cm^2$. The integrated intensity from the optimized ($NaYbF_4$: $Tm^{3+}$ 0.5%)@$NaYF_4$: $Nd^{3+}$ 30% core/shell sample is evaluated to be about ~ 41 times higher than that from reported highly efficient ($NaYF_4$:$Yb^{3+}$ 20%, $Tm^{3+}$ 0.5%, $Nd^{3+}$ 1%)@$NaYF_4$:$Nd^{3+}$ 20% core/shell nanoparticles.[4]

## E. Supporting Figures for IR Dye-Sensitized Core/Shell Nanostructures

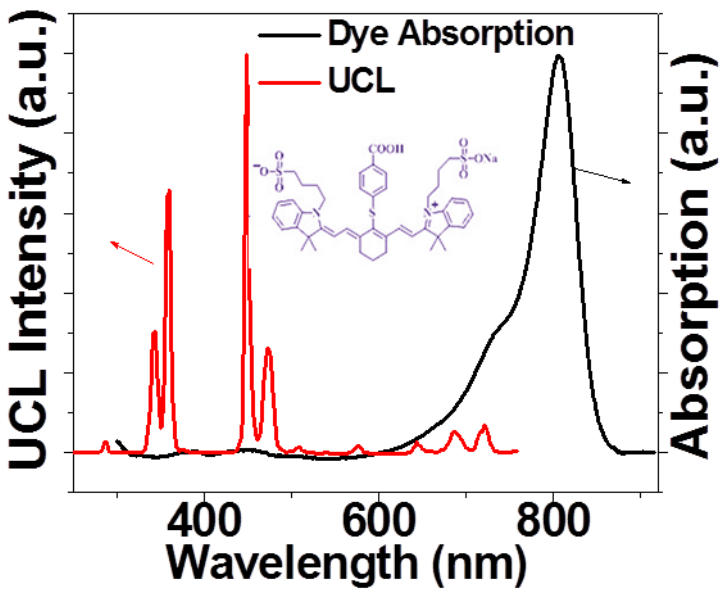


**Figure S19.** Absorption spectrum of the IR-808 dye versus the UCL spectrum of the optimized ($NaYbF_4$: $Tm^{3+}$ 0.5%)@$NaYF_4$: $Nd^{3+}$ 30% core/shell nanoparticles. The two spectra were normalized for clear comparison. The inset shows the structure of used IR-808 dye. Both the dye and the core/shell nanoparticles were dispersed in DMF.

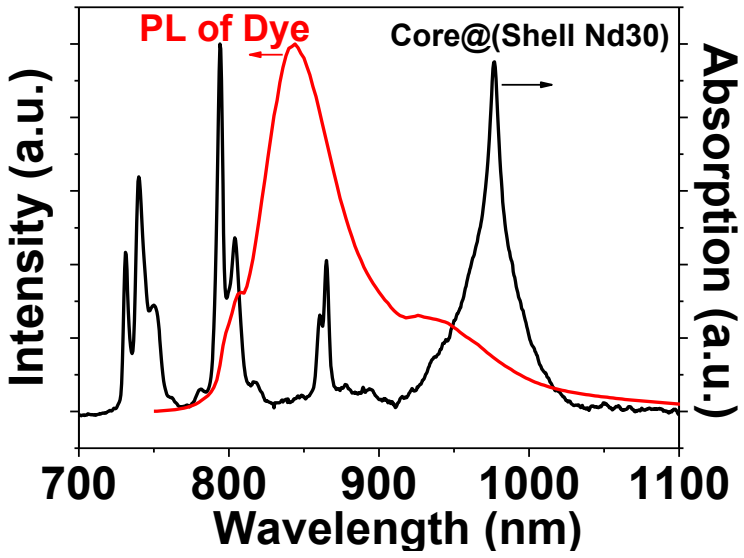


**Figure S20.** The emission spectrum of IR-808 in DMF (excitation at 800 nm) and the absorption of the ($NaYbF_4$: $Tm^{3+}$ 0.5%)@$NaYF_4$: $Nd^{3+}$ 30% core/shell nanoparticles. The peaks at 740, 800, and

860 nm correspond to the absorption of $Nd^{3+}$ ions in the shell, while the peak at ~ 980 nm corresponds to the absorption of $Yb^{3+}$ ions in the core.

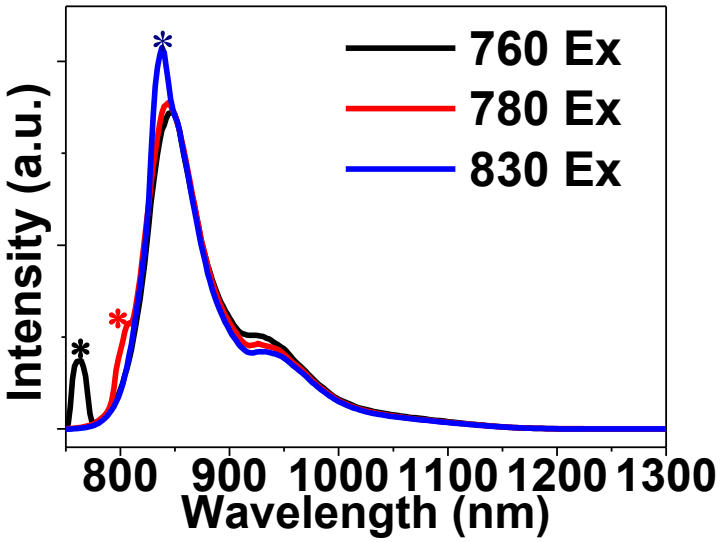


**Figure S21.** The luminescence spectra of IR-808 dye dispersed in DMF under different excitation wavelengths. No optical filters are used during the measurement. The peaks marked by asterisks are caused by the excitation light. The identical luminescence spectra of IR-808 suggest an identical mechanism of nonradiative energy transfer from the IR-808 dye to doped $Nd^{3+}$ ions, despite excitation of the dye at different wavelengths.

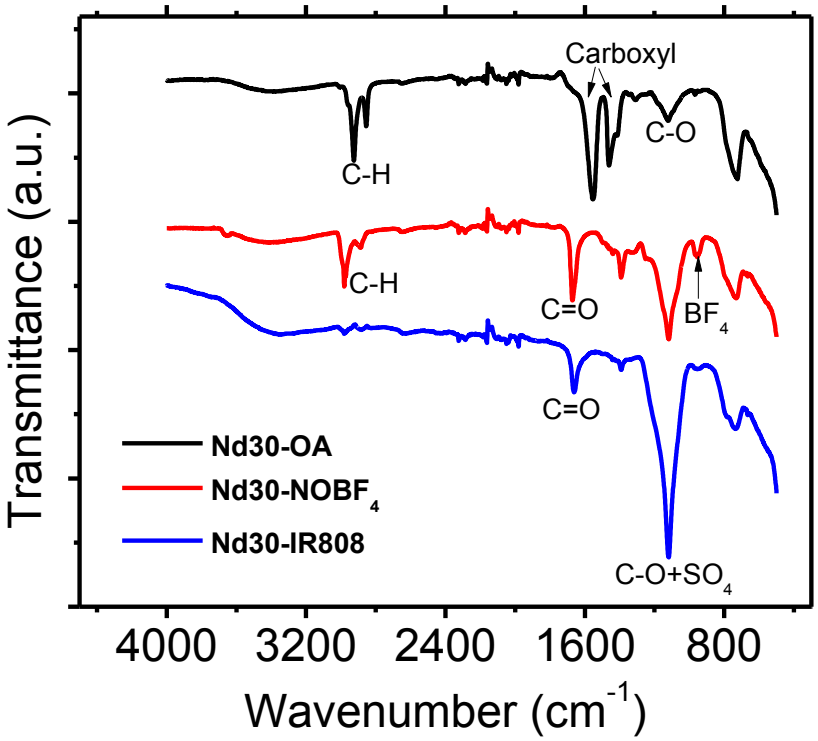


**Figure S22.** Fourier transform infrared (FTIR) spectra of the as-prepared, oleic acid (OA)-coordinated ($NaYbF_4$:Tm0.5%)/$NaYF_4$:$Nd^{3+}$30% (Nd30-OA) core/shell nanoparticles, the $NOBF_4$-coordinated ($NaYbF_4$:Tm0.5%)/$NaYF_4$:$Nd^{3+}$30% core/shell nanoparticles (Nd30-$NOBF_4$), and the IR 808-attached ($NaYbF_4$:Tm0.5%)/$NaYF_4$:$Nd^{3+}$30% core/shell nanoparticles (Nd30-IR 808). In comparison to the FTIR spectra of Nd30-OA, the FTIR spectra of Nd30-$NOBF_4$ show that the intensity of the characteristic C-H stretching vibrations at 2800-3000 $cm^{-1}$, ascribed to OA molecules, is noticeably reduced after surface treatment. Moreover, a significant reduction in the vibrational peak of the carboxyl group (1500-1200 $cm^{-1}$) is observed, along with the appearance of vibrational peak of $BF_4$ group (1084 $cm^{-1}$). These observations confirm a successful ligand exchange of $NOBF_4$ with the OA ligand on the as-prepared nanoparticle surface. The new peak around 1650 $cm^{-1}$ can be attributed to C=O stretching vibrations of the solvent DMF molecules, while the broad band around 3500 $cm^{-1}$ is assigned to the solvated water molecules. When further treated with the IR 808 dye, the vibrational peak at ~ 1000 $cm^{-1}$ intensifies about 3 times and its shape changes, due to the interaction of the sulfate group with the surface. The existed vibration peaks of the sulfate group, in conjunction with the vibrations of the carboxylic group (1500-1200 $cm^{-1}$), suggest that IR 808 dyes are anchored on the nanoparticle surface through both the sulfate and the carboxylic groups.

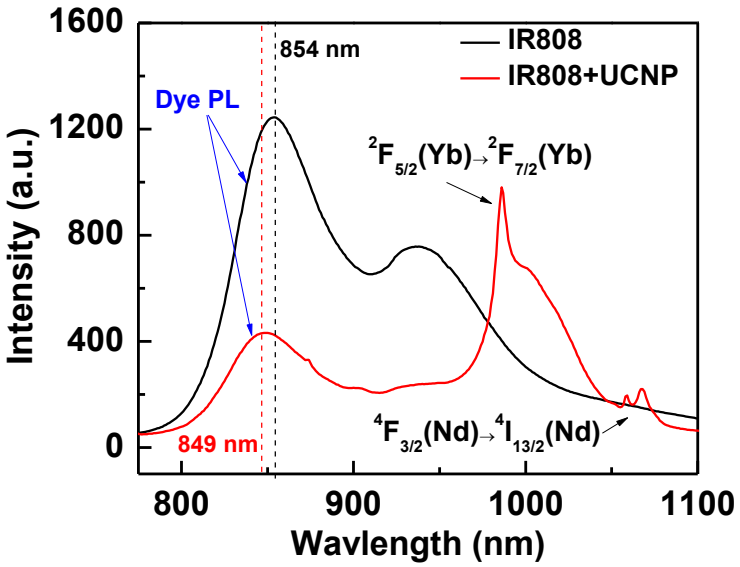


**Figure S23.** A comparison of luminescence spectra of IR-808 in a free pure dye solution (dispersed in DMF) and in a dye-attached ($NaYbF_4$: $Tm^{3+}$ 0.5%)@$NaYF_4$: $Nd^{3+}$ 30% core/shell upconverting nanoparticle solution (dispersed in DMF) under laser excitation at 750 nm. The fluorescence peak was shifted from 854 to 849 nm when IR-808 were bound to the surface of the ($NaYbF_4$: $Tm^{3+}$ 0.5%)@$NaYF_4$: $Nd^{3+}$ 30% core/shell nanoparticles. Moreover, the appearance of strong downconversion luminescence (DCL) of $Yb^{3+}$ ions and weak DCL of $Nd^{3+}$ ions, along with a significant decrease of dye fluorescence, indicates an efficient energy transfer from IR 808 dye on the surface to the $Nd^{3+}$ ions in the shell, and then to the $Yb^{3+}$ ions in the core.

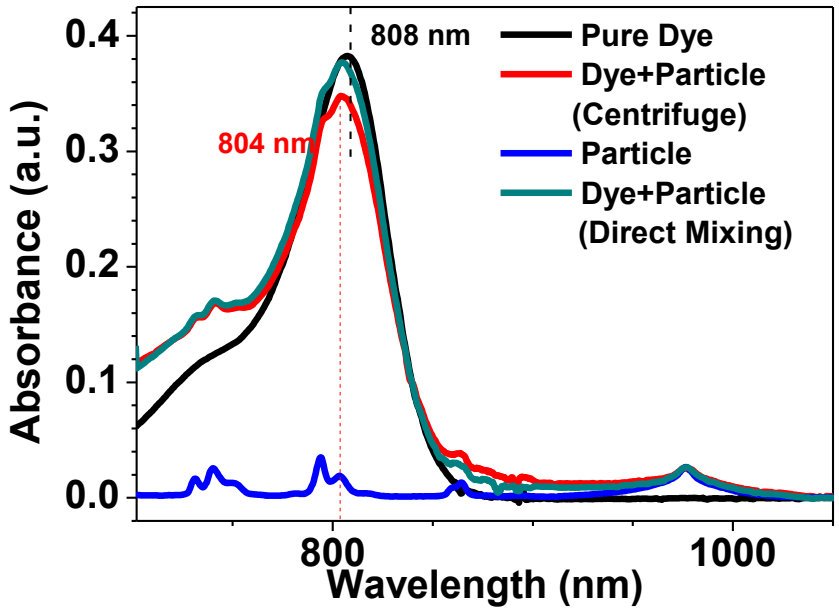


**Figure S24.** Absorption spectra of pure IR-808 dye, IR-808-attached ($NaYbF_4$: $Tm^{3+}$ 0.5%) @ $NaYF_4$: $Nd^{3+}$ 30% core/shell upconverting nanoparticles (before and after centrifuging purification), as well as ($NaYbF_4$: $Tm^{3+}$ 0.5%) @ $NaYF_4$: $Nd^{3+}$ 30% core/shell upconverting nanoparticle. All three samples are dispersed in DMF for measurement. The maximum absorption wavelength of IR-808 was blue-shifted from 808 nm in pure dye solution to 804 nm in the dye-attached core/shell upconverting nanoparticles. Absorption spectra of IR-808-attached ($NaYbF_4$: $Tm^{3+}$ 0.5%) @ $NaYF_4$: $Nd^{3+}$ 30% core/shell upconverting nanoparticles before and after purification with centrifugation indicate that over 92—97% IR-808 dyes remain on the nanoparticle surface, close to 100%. The mass coefficients, molar coefficients, and absorption cross sections of these three samples were determined using Beer-Lambert law, and listed in Table S4.

**Table S4.** Optical parameters and molar mass of IR-808 dye, ($NaYbF_4$: $Tm^{3+}$ 0.5%) @ $NaYF_4$: $Nd^{3+}$ 30% nanoparticles, and IR-808-attached ($NaYbF_4$: $Tm^{3+}$ 0.5%) @ $NaYF_4$: $Nd^{3+}$ 30% core/shell upconversion nanoparticles.

| **Optical Parameters** | | | |
|---|---|---|---|
| | **dye only** | **UCNP only** | **UCNP+dye (centrifuge)** |
| **Absorption Peak** | 808 nm | 794 nm | 804 nm |
| **Mass Extinction Coefficient** | 12.4 l $g^{-1}$ $cm^{-1}$ | 4.2x$10^{-3}$ l $g^{-1}$ $cm^{-1}$ | *** |
| **Molar Extinction coefficient** | 10746 $M^{-1}cm^{-1}$ | 890480 $M^{-1}cm^{-1}$ | 8841029 $M^{-1}cm^{-1}$ |
| **Absorption cross section** | 1.78x$10^{-17}$ $cm^2$ | 1.48 x$10^{-15}$ $cm^2$ | 1.47x$10^{-14}$ $cm^2$ |
| **Molar Mass dye** | 843.3 g/mol | | |
| **Molar Mass UCNP** | 2.11x$10^8$ g/mol | | |
| **Number of dye per UCNP** | 830 | | |

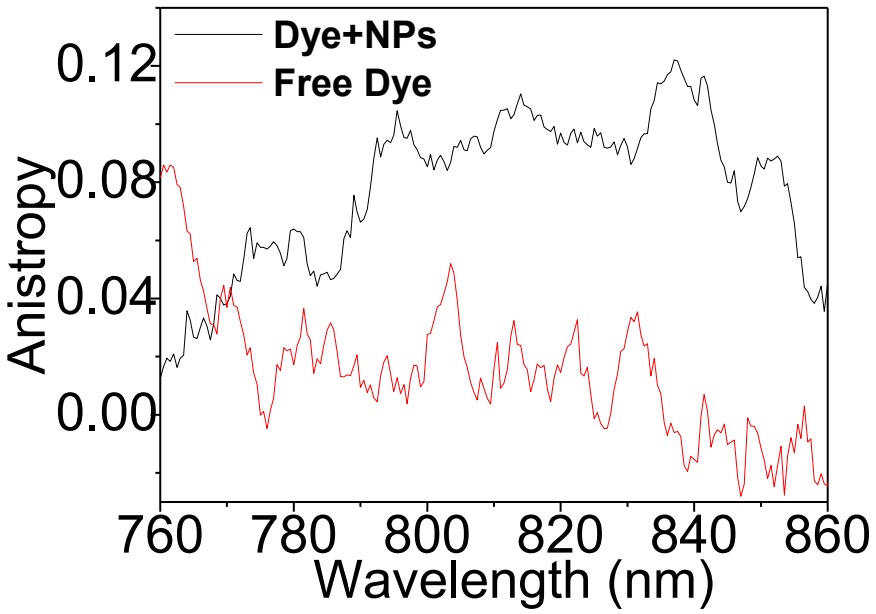


**Figure S25.** Fluorescence anisotropy of IR-808 in a free dye solution and in a mixture of dye and $NOBF_4$-coated ($NaYbF_4$: $Tm^{3+}$ 0.5%) @ $NaYF_4$: $Nd^{3+}$ 30% core/shell upconversion nanoparticles. Fluorescence anisotropy in a spectrofluorometer is defined as $r = (I_{VV} - GI_{VH})/(I_{VV} + 2GI_{VH})$, where $I_{VV}$, $I_{VH}$, $I_{HV}$, and $I_{HH}$ are emission intensities for different positions of excitation and emission polarizers; the first subscript indicates the position of the excitation polarizer, the second that of the emission polarizer. $G = I_{HV}/I_{HH}$ is a grating factor that must be included for correction in a monochromator.[8] The free IR-808 dye solution exhibits zero anisotropy, while the fluorescence of IR-808 in the presence of $NOBF_4$-coated core/shell nanoparticles shows an increased anisotropy. This is understandable because the rotational mobility of dye molecules is restricted when they are bound to the surface of the nanoparticles.[8-9]

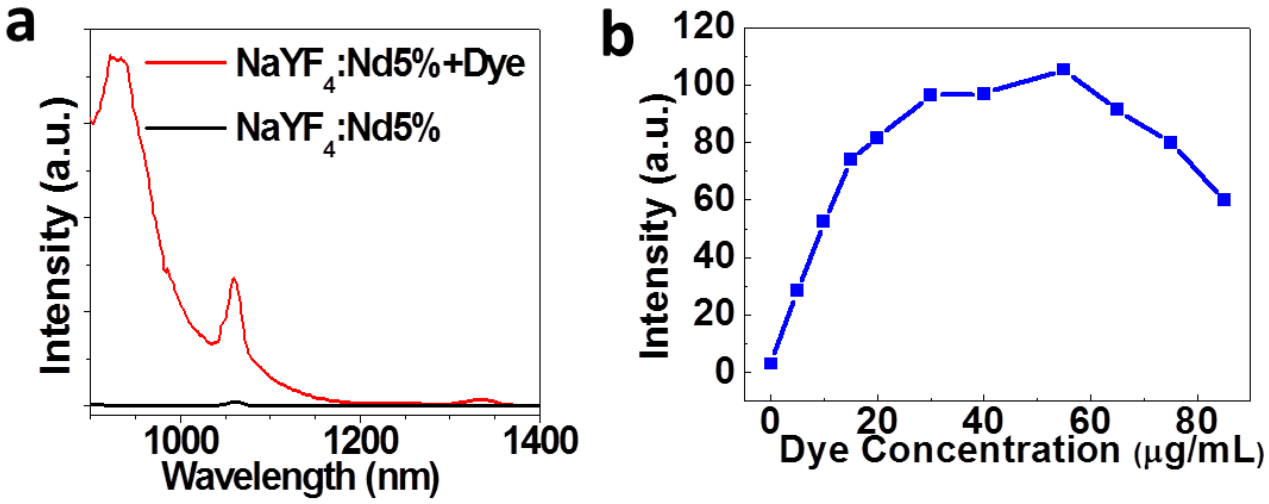


**Figure S26. a,** Luminescence spectra of 30 nm sized $NaYF_4$:$Nd^{3+}$5% nanoparticles with and without sensitization by IR-808 (DMF dispersion). **b**, The intensity of luminescence at ~1050 nm (corresponding to the $^4F_{3/2} \rightarrow {}^4I_{11/2}$ transition of $Nd^{3+}$) from $NaYF_4$: $Nd^{3+}$ nanoparticles versus the concentration of IR-808 dye (DMF dispersion, excited at 800 nm, ~ 2 W/cm$^2$). The luminescence was significantly enhanced due to the presence of IR-808; the maximum enhancement reaches 33 fold at an optimal dye concentration of ~ 30-50 μg/mL. This result verifies the existence of efficient energy transfer process from IR-808 to $Nd^{3+}$ ions in a fluoride host lattice.

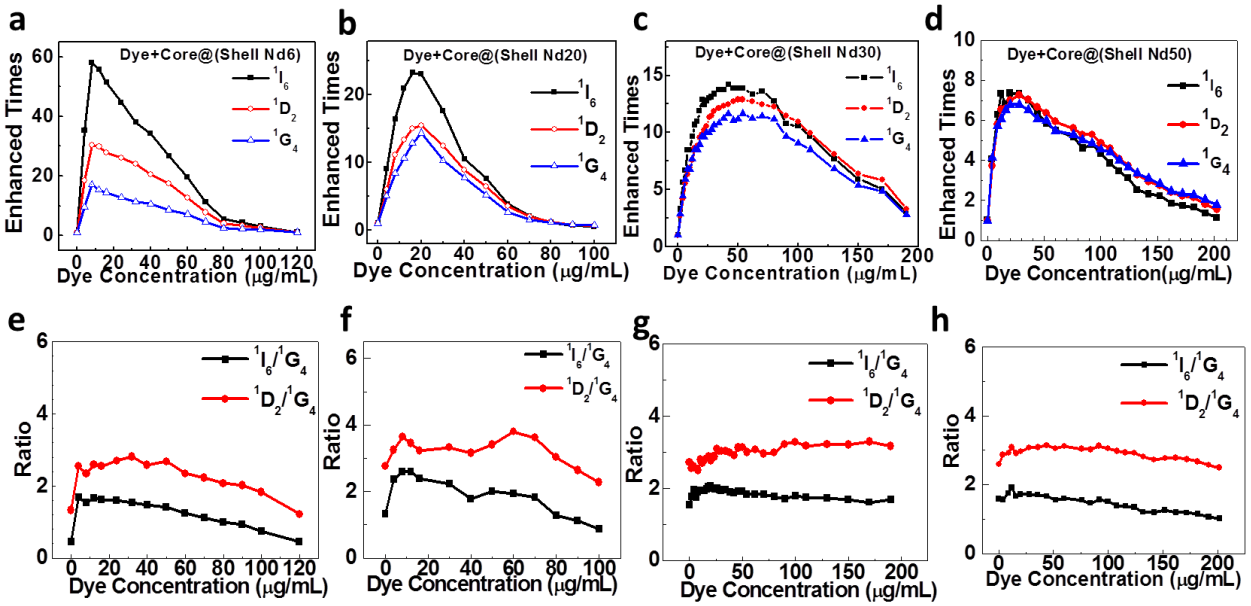


**Figure S27. (a-d)** The enhancement of the UCL from the $^1I_6$, $^1D_2$, $^1G_4$ states of $Tm^{3+}$ ions in the core/shell ($NaYbF_4$: $Tm^{3+}$ 0.5%)@$NaYF_4$: $Nd^{3+}$ x% (x=6, 20, 30, 50) nanoparticles versus the IR-808 dye concentration. **(e-f)** The ratios of luminescence intensities for the $^1I_6/^1G_4$ and the $^1D_2/^1G_4$

states in the core/shell ($NaYbF_4$: $Tm^{3+}$ 0.5%)@$NaYF_4$: $Nd^{3+}$ x% (x=6, 20, 30, 50) nanoparticles versus the IR-808 dye concentration. The excitation is performed at 800 nm, 10 W/cm$^2$. The UCL enhancement from all these three states in all samples exhibit a similar dependence behavior on the IR-808 dye concentration, revealing ~8-60 fold enhancement at an optimal dye concentration of ~ 10-30 μg/mL. The enhancement decreases with an increase in $Nd^{3+}$ concentration in the shell, while the optimal dye concentration increases with the $Nd^{3+}$ concentration. The ratios of intensities of luminescence from the $^1I_6/^1G_4$ and the $^1D_2/^1G_4$ states are increased with an addition of the IR-808 dye, and then remain almost independent of $Nd^{3+}$ concentration and the IR-808 dye concentration, which correlates with the fact that UC processes are saturated at laser irradiance of 10 W/cm$^2$ (consult Fig. S30). These results indicate that the enhancement of mulitphoton UCL is mainly caused by the increase of absorption at the excitation wavelength due to IR-808 presence.

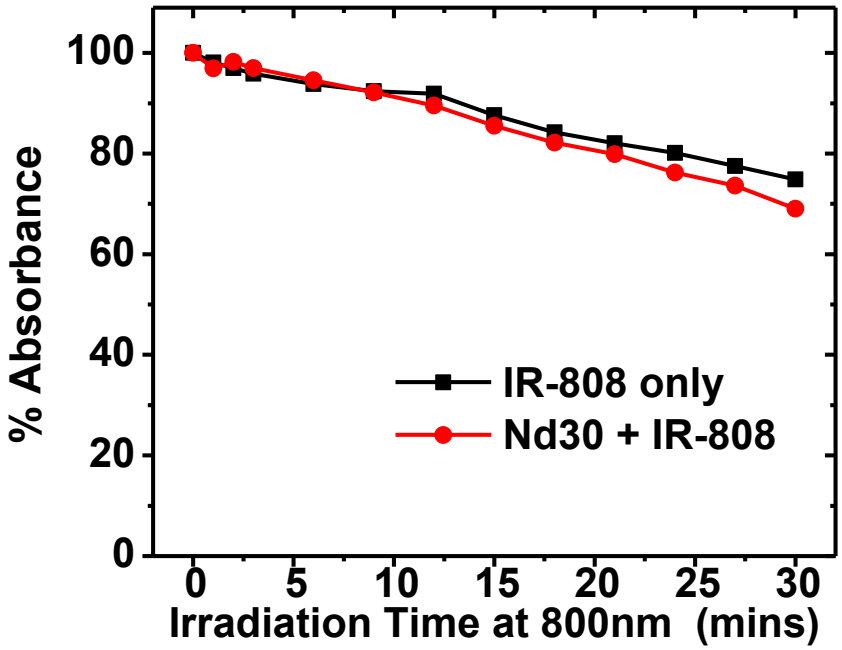


**Figure S28.** Evaluation of the photostabilities of IR-808 dye associated with/ ($NaYbF_4$:Tm0.5%)/$NaYF_4$:$Nd^{3+}$30% UCNPs (Nd30+IR 808) and the free dye. DMF was used as the solvent; laser irradiation at 800 nm with power density of ~5 W/cm$^2$

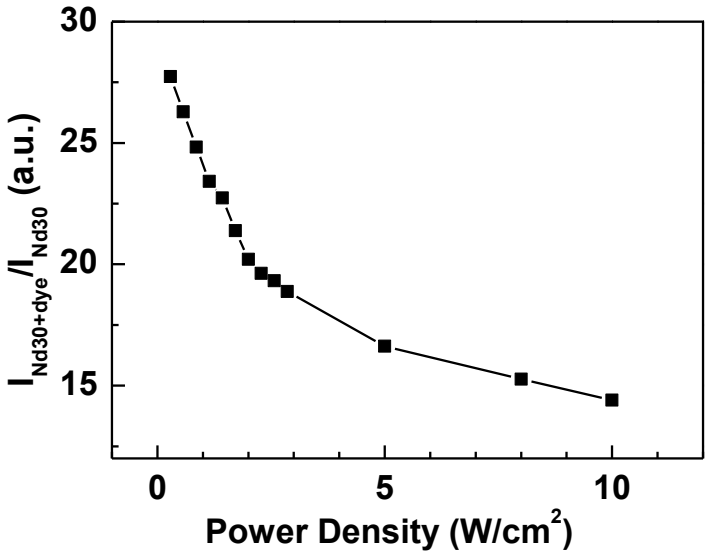


**Figure S29.** The enhancement of integrated UCL in IR-808-sensitized core/shell ($NaYbF_4$: $Tm^{3+}$ 0.5%)@$NaYF_4$: $Nd^{3+}$ 30% nanoparticles (at an optimal dye concentration of 30 μg/mL) as a function of laser excitation power density. Much more pronounced enhancement folds are observed at low excitation power density range, reaching 28-fold at 800 nm of ~0.3 W/cm$^2$. This is due to different power dependencies for UCL from nanoparticles only and in combination with dye.

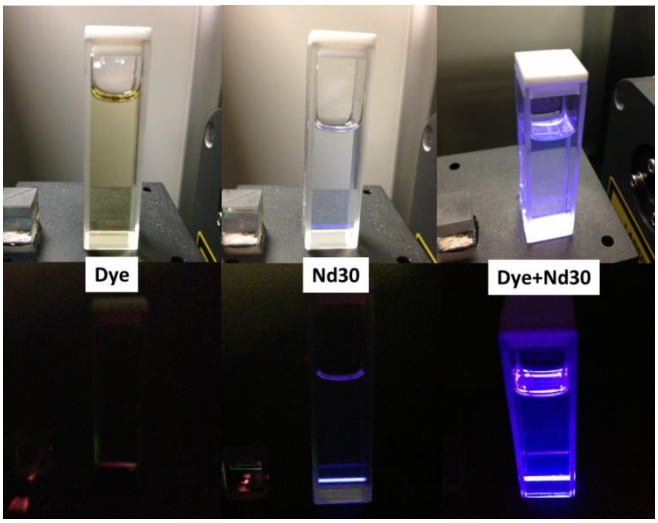


**Figure S30.** Photographic images of free IR-808 dye, core/shell ($NaYbF_4$: $Tm^{3+}$ 0.5%)@$NaYF_4$: $Nd^{3+}$ 30% nanoparticles, as well as IR-808-sensitized core/shell ($NaYbF_4$: $Tm^{3+}$ 0.5%)@$NaYF_4$: $Nd^{3+}$ 30% nanoparticles (dye concentration 100 μg/mL) taken under plain lighting and dark background (excited at ~ 800 nm, 1 W/cm$^2$). A much stronger UCL was observed from IR-808 sensitized core/shell nanoparticles than the pure core/shell nanoparticles, confirming the importance of sensitization.

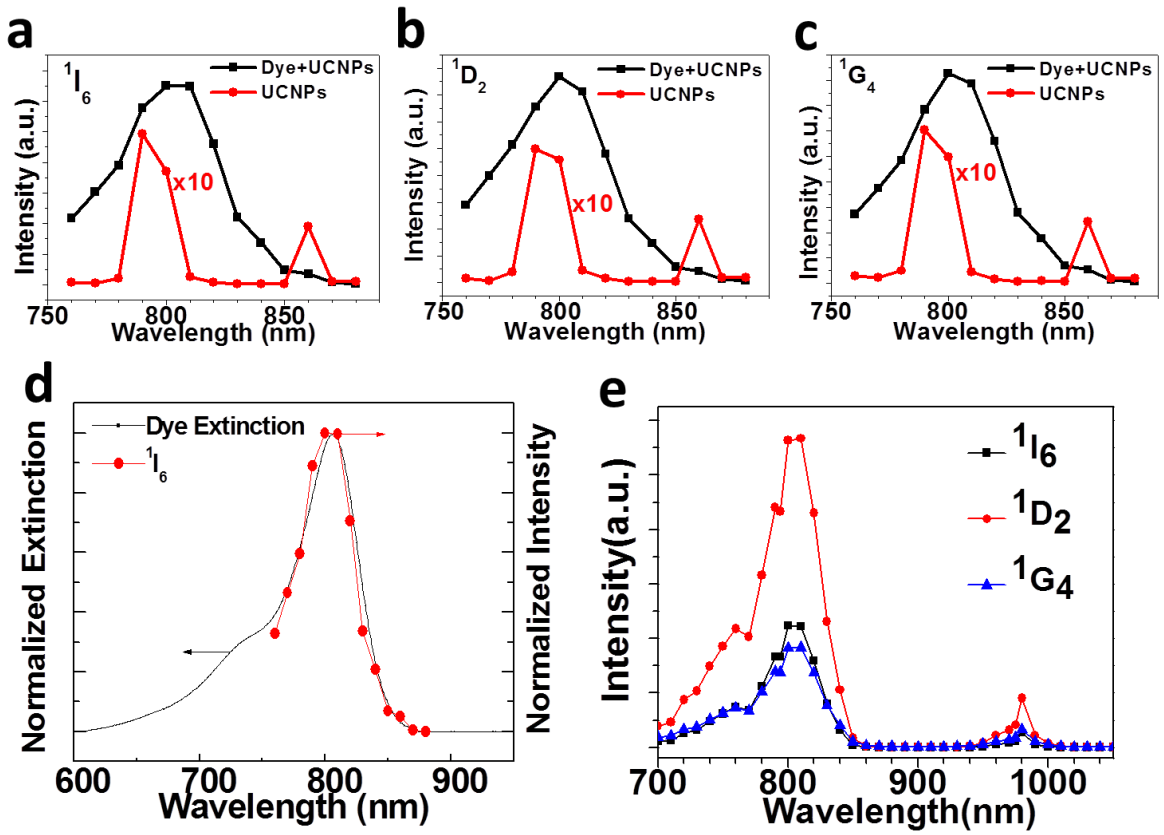


**Figure S31. (a-c)** The excitation spectra of UCL from the $^1I_6$, $^1D_2$, $^1G_4$ states, respectively, of $Tm^{3+}$ ions from the core/shell ($NaYbF_4$: $Tm^{3+}$ 0.5%)@$NaYF_4$: $Nd^{3+}$ 30% nanoparticles as well as IR-808-sensitized core/shell ($NaYbF_4$: $Tm^{3+}$ 0.5%)@$NaYF_4$: $Nd^{3+}$ 30% nanoparticles. **(d)** A comparison of the excitation spectra from the $^1I_6$ state and the extinction (or absorption) spectra of IR-808 dye. **(e)** The excitation spectra in of UCL from the $^1I_6$, $^1D_2$, $^1G_4$ states in a broader range (700-1100 nm) from IR-808-sensitized core/shell ($NaYbF_4$: $Tm^{3+}$ 0.5%)@$NaYF_4$: $Nd^{3+}$ 30% nanoparticles. The excitation was provided by a femtosecond Ti: Sapphire laser (Chameleon from Coherent). The obtained spectra in (e) match the corresponding spectral result in (a-c) in the wavelength range of 760-870 nm, confirming that the independence of excitation spectra of the excitation laser pulse width.

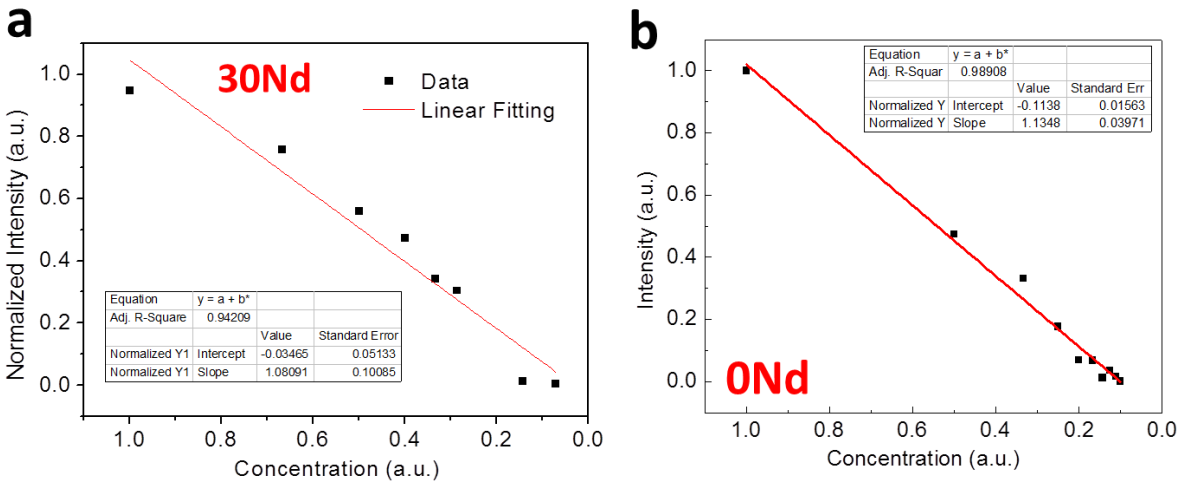


**Figure S32.** The dependence of the integrated UCL from the $^1D_2$ state of $Tm^{3+}$ ions of the IR-808 sensitized ($NaYbF_4$: $Tm^{3+}$ 0.5%)@$NaYF_4$ and ($NaYbF_4$: $Tm^{3+}$ 0.5%)@$NaYF_4$: $Nd^{3+}$ 30% core/shell nanoparticles on the diluted sensitized nanoparticle concentration. A linear dependence is observed for both samples, ruling out the possibility of luminescence mediated energy transfer.

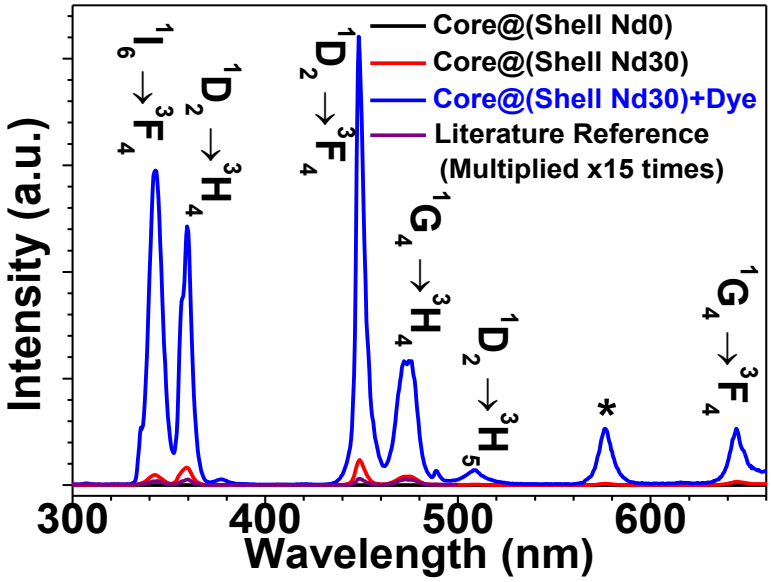


**Figure S33.** UCL spectra of ($NaYbF_4$: $Tm^{3+}$ 0.5%)@$NaYF_4$ (black line), ($NaYbF_4$: $Tm^{3+}$ 0.5%)@$NaYF_4$: $Nd^{3+}$ 30% (red line), dye-sensitized ($NaYbF_4$: $Tm^{3+}$ 0.5%)@$NaYF_4$: $Nd^{3+}$ 30% (blue line), and the recently reported as record high efficient ($NaYF_4$:$Yb^{3+}$ 20%, $Tm^{3+}$0.5%, $Nd^{3+}$1%)@$NaYF_4$:$Nd^{3+}$ 20% (purple line) core/shell nanoparticles. UCNPs were compared using the same concentration dispersed in DMF. Excitation at 800 nm, 10 W/cm$^2$.

## F. Estimations of Molecular Weights, Number of Dyes per Core/Shell Nanoparticle, and Intermolecular Distance of NIR Dye on the Surface of a Core/Shell nanoparticle

***Molecular weight of the core-shell nanoparticles:*** The 50 nm oleic-acid coated ($NaYbF_4$: $Tm^{3+}$ 0.5%) @ $NaYF_4$: $Nd^{3+}$ 30% core/shell nanoparticle has a 30 nm sized core and a 10 nm thickness of shell. The volume of the core and shell were determined by a spherical approximation. We then follow the same protocol reported in our recent work,[10] and estimate the molecular weight of the core-shell upconversion nanoparticles to be $2.1 \cdot 10^8 g/mol$.

***Number of dye per core/shell nanoparticles:*** The number of IR-808 dye per ($NaYbF_4$: $Tm^{3+}$ 0.5%) @ $NaYF_4$: $Nd^{3+}$ 30% core/shell nanoparticle was determined to be ~ 830, according to the number of bound IR-808 dye (32.61 nmol, calculated from the weight of 27.5 μg), and the amount of ($NaYbF_4$: $Tm^{3+}$ 0.5%) @ $NaYF_4$: $Nd^{3+}$ 30% core/shell nanoparticle (~0.0393 nmol, calculated from the nanoparticle weight of 8300 μg). The amount of dye was estimated by using the added weight of the dye as well as its molecular weight, assuming that nearly all the added dye molecules are attached to the nanoparticle surface.

***Intermolecular distance of IR-808 dye on the surface of a core/shell nanoparticle:*** At the optimal number of IR-808 dye per core/shell nanoparticle, the surface coverage of a ($NaYbF_4$: $Tm^{3+}$ 0.5%) @ $NaYF_4$: $Nd^{3+}$ 30% core/shell nanoparticle (diameter ~ 50 nm, 7853.98 $nm^2$) will determine an average "effective" area of ~ 9.46 $nm^2$ per dye. This value will result in average center-to-center distance of ~3 nm for IR-808 dye at the optimal dye concentration.

**G. Quantification of Upconversion Quantum Efficiency and Pump Power Dependence.**

The upconversion quantum efficiency (QE) is defined as the fraction of the absorbed photons that serve to generate upconversion emissions.[11,12] This parameter precisely defines the upconverting ability of the characterized materials. The upconversion quantum yield (QY) of luminescence is known as the ratio of the number of the emitted photons to the number of the absorbed photons. The upconversion QE and upconversion QY can be related:

$$QE_{UC} = \sum_i i * QY_{UCi} \quad \text{(S2)}$$

where i is the number of the absorbed photons to produce $i^{th}$ multiphoton upconversion emissions and $QY_{UCi}$ represents the quantum yield of $i^{th}$ multiphoton upconversion emissions. The upconversion QY can be measured either by absolute method or on a relative basis, using standard with known QY as a reference. Here, we determined the $QY_{UCi}$ of our samples by referencing to the standard indocynine green dye in DMSO with a known quantum yield of 12%. The determination of QY (for the $i^{th}$ multiphoton upconversion emissions) follows exactly the procedure from our recent report using the following equation,[3]

$$QY_{UC} = QY_{ref}\left(\frac{E_{UC}}{E_{ref}}\right)\left(\frac{A_{ref}}{A_{UC}}\right)\left(\frac{I_{ref}}{I_{UC}}\right)\left(\frac{n_{UC}}{n_{ref}}\right)^2 \quad \text{(S3)}$$

Where $E_{UC}$ and $E_{ref}$ are the numbers of the emitted photons for referenced standard sample and measured sample, respectively; $A_{ref}$ and $A_{UC}$ are the numbers of the photons absorbed by referenced standard sample and measured sample, respectively, $I_{ref}$ and $I_{UC}$ indicate the relative intensity of the exciting light for referenced standard sample and measured sample, respectively; $n_{UC}$ and $n_{ref}$ are the average refractive index of the solvent used for dissolving referenced standard sample and measured sample, respectively. A matching of the absorption of measured upconverting sample and reference standard was used along with an employment of identical luminescence excitation and recording geometry. This greatly simplified the quantification process of upconversion quantum efficiency shown in Figure S29.

The upconversion quantum efficiencies of dye-sensitized $NaYF_4:Yb^{3+}/Er^{3+}$ nanoparticles (Ref. 16 in the main text) and the core/shell/shell nanostructure $NaYF_4:Yb^{3+}20\%,Er^{3+}2\%$ @$NaYF_4:Yb^{3+}10\%$ @ $NaNdF_4:Yb^{3+}10\%$ (Ref. 26 in the main text) have been calculated using the determined two-photon processes for visible emissions.

This measured upconversion QY can be converted into the upconversion energy conversion efficiency (UCECE) or the upconversion efficiency (UCE) by considering the energy of the photons ($E_\lambda = hc/\lambda$) in the emission and excitation spectra, where h is Planck's constant, c is the speed of light, and $\lambda$ the wavelength.

$$ECE_{UC} = QY_{UC}\left(\frac{\lambda_{Exciation}}{\lambda_{Emission}}\right) \quad \text{(S4)}$$

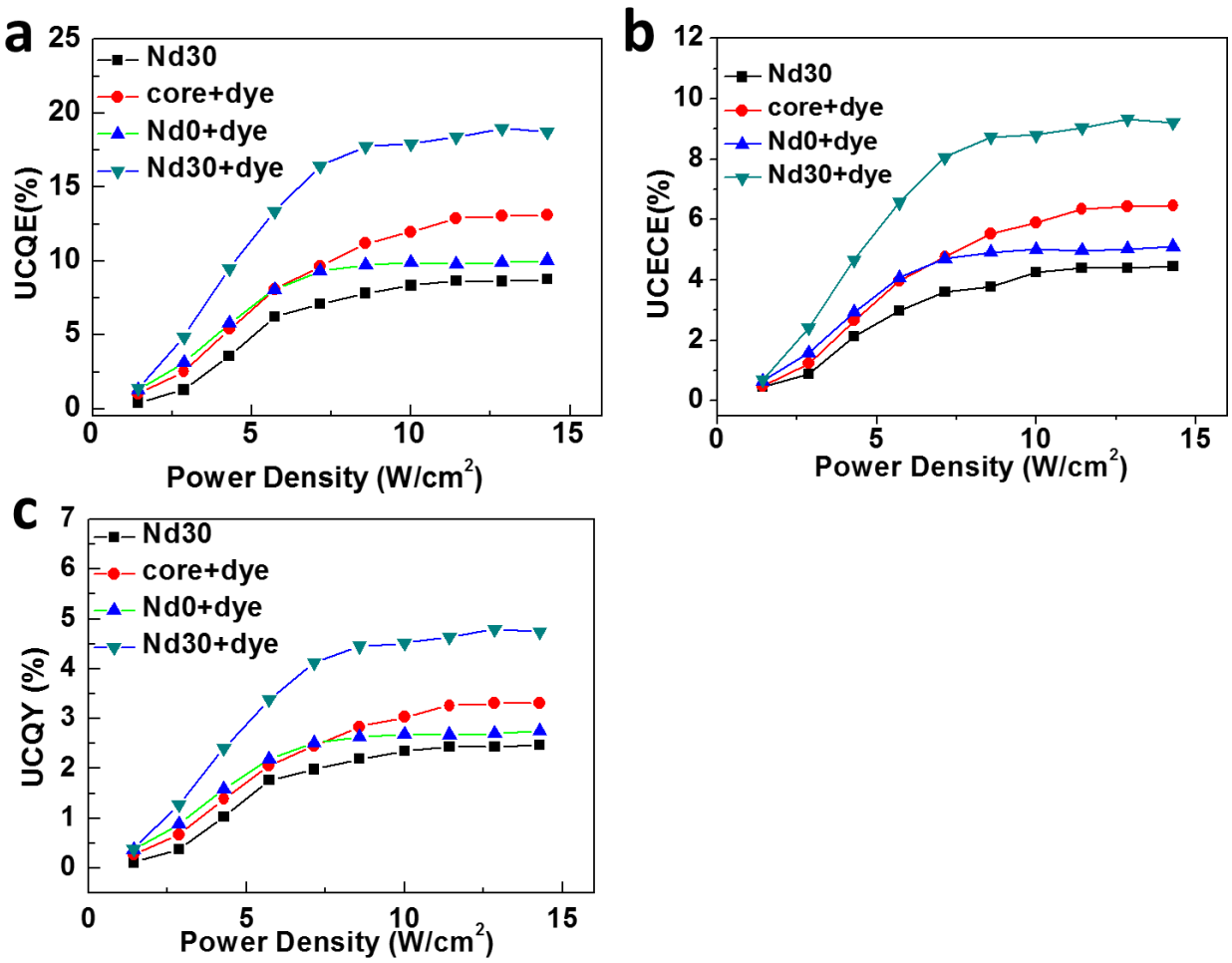


**Figure S34. a,** The upconversion quantum efficiency (UCQE), **b**, The upconversion energy conversion efficiency (UCECE) or upconversion efficiency (UCE), and **c**, The conventional upconversion quantum yield (UCQY), of ($NaYbF_4$: $Tm^{3+}$ 0.5%)@$NaYF_4$: $Nd^{3+}$ 30% nanoparticles (Nd30), IR-808 sensitized $NaYbF_4$: $Tm^{3+}$ 0.5% nanoparticles (IR-808 + core), IR-808 sensitized ($NaYbF_4$: $Tm^{3+}$ 0.5%)@$NaYF_4$ (Nd 0+IR-808) nanoparticles, and IR-808 sensitized ($NaYbF_4$: $Tm^{3+}$ 0.5%)@$NaYF_4$: $Nd^{3+}$ 30% (Nd 30+IR-808) nanoparticles versus the excitation power density. As illustrated, the UCQE of all samples increase along with an increase of laser excitation power density, but reach a plateau at around 8-10 W/cm$^2$ due to the occurrence of a saturation effect. The IR-808 sensitized ($NaYbF_4$: $Tm^{3+}$ 0.5%)@$NaYF_4$: $Nd^{3+}$ 30% core/shell nanoparticles have the highest upconversion quantum efficiency among all excitation range, reaching a value of ~19% above 10 W/cm$^2$. Their corresponding upconversion energy conversion efficiency (or upconversion efficiency) and upconversion quantum yield are determined to be ~ 9.3% and ~ 4.8%, respectively.

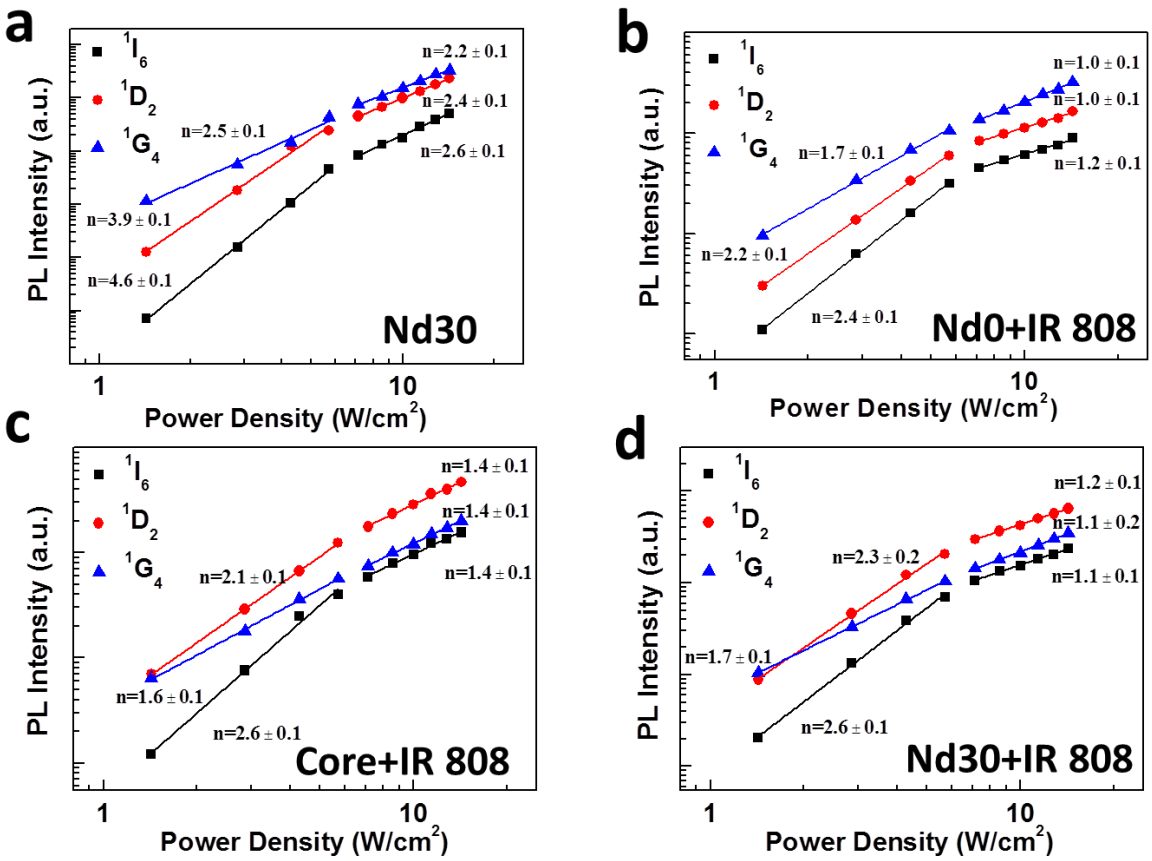


**Figure S35.** The dependence of the intensities of upconverted luminescence from the $^1I_6$, $^1D_2$, $^1G_4$ states of $Tm^{3+}$ ions from ($NaYbF_4$: $Tm^{3+}$ 0.5%)@$NaYF_4$: $Nd^{3+}$ 30% (Nd30, **a**), IR-808 sensitized ($NaYbF_4$: $Tm^{3+}$ 0.5%)@$NaYF_4$ (Nd 0+IR-808, **b**), IR-808 sensitized $NaYbF_4$: $Tm^{3+}$ 0.5% (IR-808 + core, **c**), and IR-808 sensitized ($NaYbF_4$: $Tm^{3+}$ 0.5%)@$NaYF_4$: $Nd^{3+}$ 30% (Nd 30+IR-808, **d**) nanoparticles on the excitation power density. The number of photons which are required to populate the upper emitting state under unsaturated condition can be obtained by the relation,[10]

$$I_f \propto P^n \qquad \text{(S4)}$$

where $I_f$ is the luminescence intensity, P is the pump laser power, and n is the number of laser photons required. Slope values of 2.5, 3.6, and 4.6 for an unsaturated situation below 6 W/cm$^2$ in ($NaYbF_4$: $Tm^{3+}$ 0.5%)@$NaYF_4$: $Nd^{3+}$ 30% nanoparticles determine that three-, four-, and five photon processes are involved to populate the $^1G_4$, $^1D_2$, and $^1I_6$ state, respectively. This result agrees well with that from previous reports.[1,4] However, saturation effects take place for all IR-808 sensitized samples and for all laser power excitation range. Slope values close to n=1 are observed for all the emitting states of all IR-808 sensitized samples. These results illustrate that the upconverting rate at each intermediate state is significantly higher than its decay rate,[13] in line with the observed high upconversion quantum efficiency in Figure S34.

## H. Supporting Figures for Generalization of Dye-Sensitized Core/Shell Structure

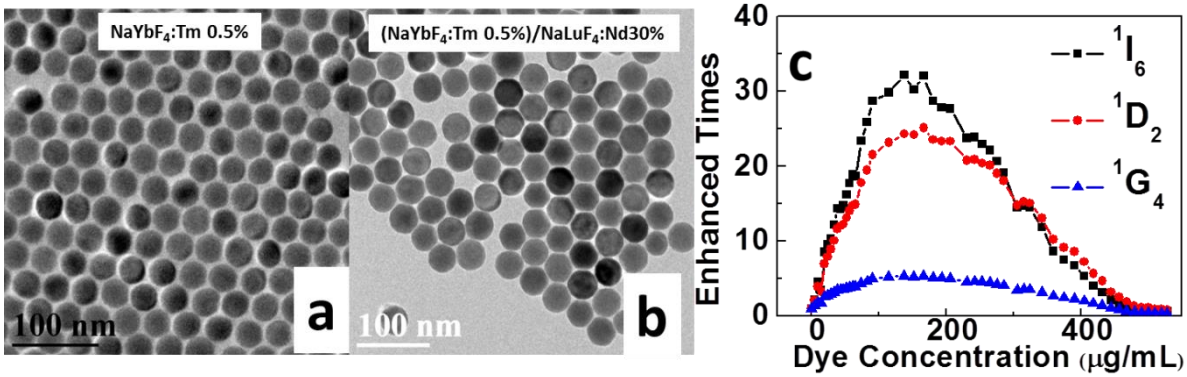


**Figure S36.** TEM micrographic images of (**a**) β-$NaYbF_4$: $Tm^{3+}$ 0.5% core nanoparticle and (**b**) β-($NaYbF_4$: $Tm^{3+}$ 0.5%)@ $NaLuF_4$: $Nd^{3+}$ 30% core/shell nanoparticles. (**c**) The enhancement folds of mulitphoton UCL from the $^1I_6$, $^1D_2$, $^1G_4$ states of the $Tm^{3+}$ ions of the β-($NaYbF_4$: $Tm^{3+}$ 0.5%)@ $NaLuF_4$: $Nd^{3+}$ 30% core/shell nanoparticles as a function of IR-808 dye concentration. More than 30 folds were observed due to IR-808 dye sensitization of the β- ($NaYbF_4$: $Tm^{3+}$ 0.5%)@ $NaLuF_4$: $Nd^{3+}$ 30% core/shell nanostructure.

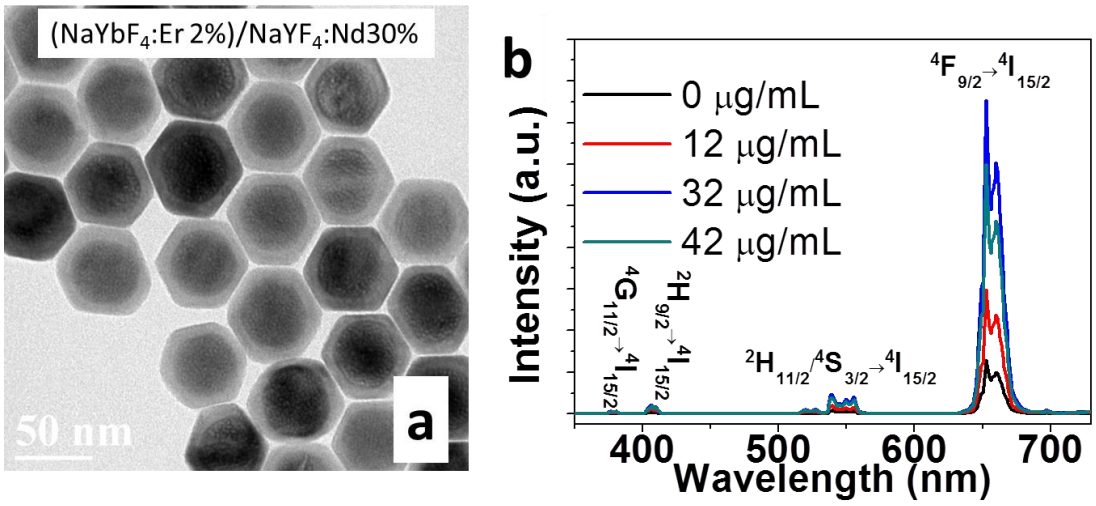


**Figure S37. a**, TEM image of β- ($NaYbF_4$: $Er^{3+}$ 2%)@ $NaYF_4$: $Nd^{3+}$ 30% core/shell nanoparticles. **b**, UCL spectra from core/shell nanoparticles in (a) with varied concentration of IR-808 dye for sensitization. The red upconversion of $Er^{3+}$ ions at 650 nm (corresponding to the $^4F_{9/2}\rightarrow{}^4I_{15/2}$ transition) is enhanced up to ~ 9 fold at an IR-808 dye concentration of 32 μg/mL.

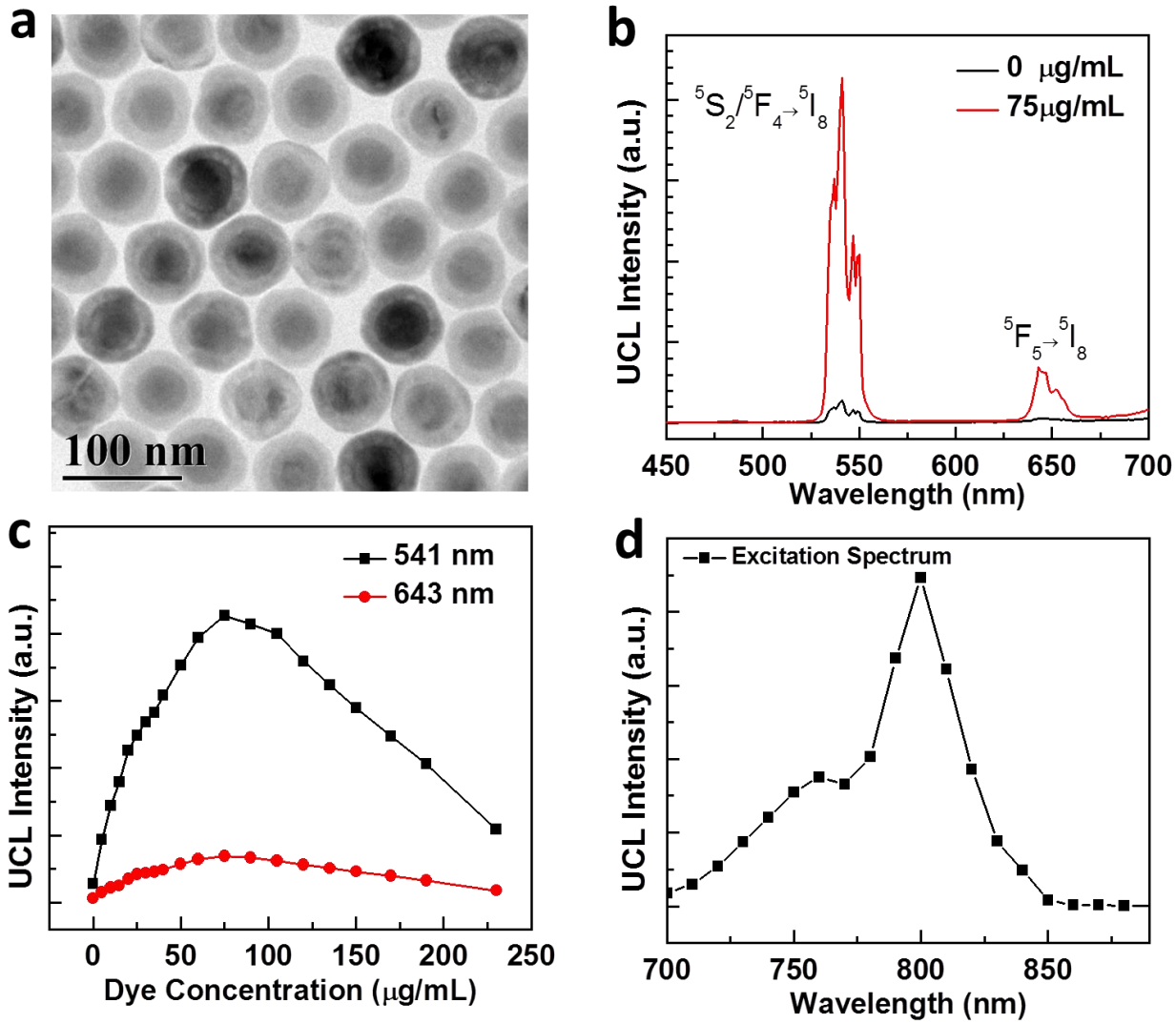


**Figure S38. a**, TEM image of β-($NaYbF_4$: $Ho^{3+}$ 2%)@ $NaYF_4$: $Nd^{3+}$ 30% core/shell nanoparticles; **b**, Compared UCL spectra from pure core/shell nanoparticles in (a) and core/shell nanoparticles with an IR-808 dye concentration of 75 μg/mL that has been optimized for sensitization effect; a 15 fold UCL enhancement was obtained (excited at 800 nm, 10 W/cm$^2$). **c**, The integrated UCL intensities of the bands at 541 and 643 nm versus varied IR-808 dye concentration, revealing an optimal dye concentration at ~75 μg/mL (excited at 800 nm, 10 W/cm$^2$); **d**, The excitation spectrum for the UCL peak at 541 nm for dye-sensitized core/shell nanoparticles; the broad band excitation peak between 700-850 nm clearly demonstrates the occurrence of a dye-sensitization effect.

## I. Supporting Figures for Applications.

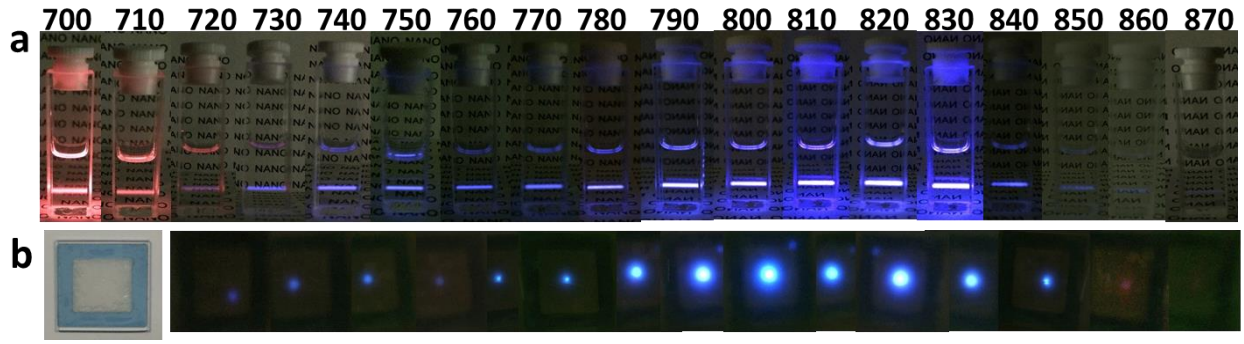


**Figure S39.** Blue upconversion emissions from IR-808 and IR-820 co-sensitized ($NaYbF_4$: $Tm^{3+}$ 0.5%)@ $NaYF_4$: $Nd^{3+}$ core/shell nanoparticles (**a**) dispersed in DMF solvent (1 wt%) and (**b**) in a polystyrene film (~30 wt%). The photographic image of home-made IR card is displayed on the left corner in b.

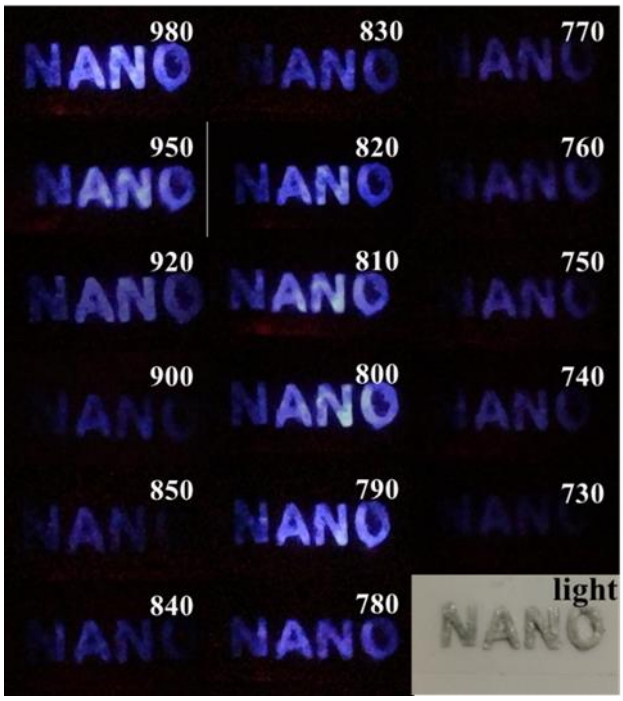


**Figure S40.** Photographic images of blue upconversion from printed letters under laser excitation with wavelength ranging from 730 to 980 nm (power density, 1 $W/cm^2$). An optical contrast image of these letters is shown in the bottom left for reference.

# J. The Theoretical Modeling

## J1. Model Energy Transfer Efficiency and Rate

We utilized the classical Förster mechanism to theoretically compare the energy transfer efficiencies between the two possible energy transfer pathways, i.e., IR-808 dye→$Nd^{3+}$→$Yb^{3+}$ and IR-808 dye→$Yb^{3+}$, to reveal the advantages of multi-step energy transfer in the designed core/shell structure whereby each step has a small energy gap. In the comparison, the distance between the IR-808 dye and the $Nd^{3+}$ (or $Yb^{3+}$) was varied from 0.5 to 6 nm, while the distance between $Nd^{3+}$ and $Yb^{3+}$ was fixed at ~ 0.353 nm, which is the lattice length of the c-axis of a hexagonal $NaYF_4$ (or $NaYbF_4$) crystal unit cell. In addition, the following parameters were utilized: the luminescence quantum yield of IR-808 dye of 0.112 (an experimental determination), the refractive index of DMF of 1.43, and the refractive index of $NaYF_4$ host lattice of ~ 1.5.

According to Förster theory, the rate between a donor-acceptor type of energy transfer can be given by the following formula,[14,15]

$$k = \frac{1}{\tau_D}(\frac{R_0}{R})^6 \quad , \tag{S5}$$

where $k$ is the energy transfer rate; $\tau_D$ is the lifetime of donor without the presence of acceptor, $R$ is the distance between donor and acceptor, while $R_0$ is the Förster radius. The Förster radius can be calculated using the formula:

$$R_0^6 = \frac{9000Q_0(\ln 10)k^2 J}{128\pi^5 n^4 N_A} \tag{S6}$$

where $Q_0$ is the luminescence quantum yield of the donor in absence of an acceptor, the $k^2$ is the dipole orientation factor (2/3 for an arbitrary orientation), $n$ is refractive index of the medium, $N_A$ is Avogadro's number, and $J$ is the spectra overlap integral which can be calculated as:

$$J = \int f_D(\lambda)\varepsilon_A(\lambda)\lambda^4 d\lambda \tag{S7}$$

Here, the $f_D(\lambda)$ is the normalized donor emission spectrum and $\varepsilon_A(\lambda)$ is the acceptor molar absorption coefficient.

The efficiency of Förster type energy transfer can be determined using the following equation:

$$E = \frac{1}{1+(R/R_0)^6} \tag{S8}$$

## 1. Evaluation of Efficiencies and Rates for IR-808 Dye→$Nd^{3+}$ and IR-808 Dye→$Yb^{3+}$ Energy Transfer Processes

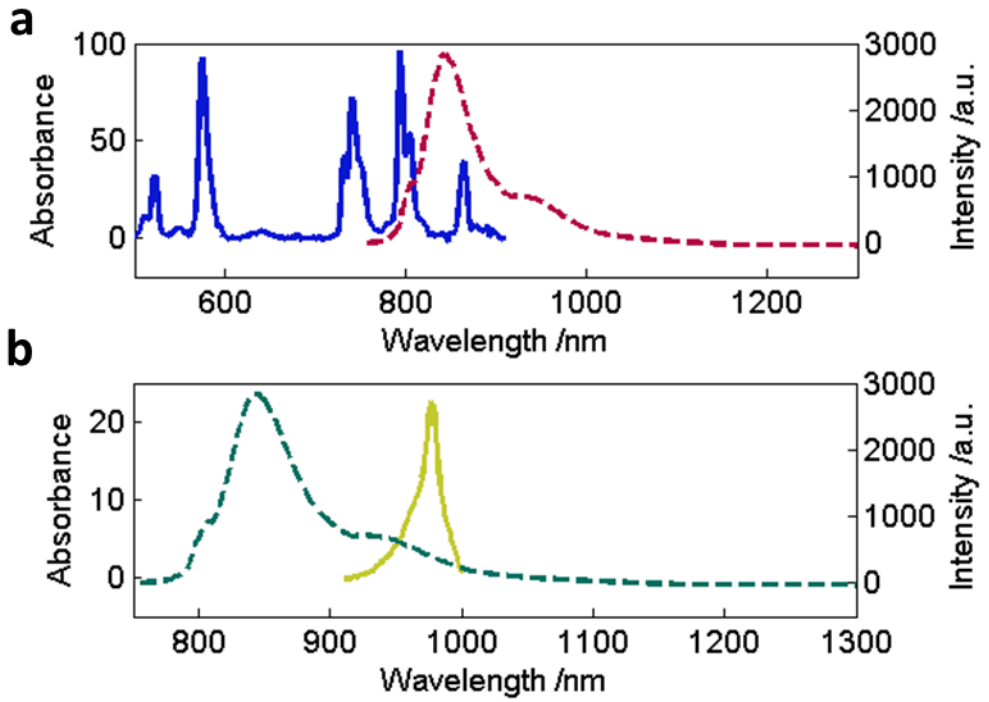


**Figure S41.** (a) The emission spectrum of the IR-808 dye donor and the absorption spectrum of $Nd^{3+}$ ions acceptor; (b) The emission spectrum of the IR-808 dye donor and the absorption spectrum of the $Yb^{3+}$ ions acceptor.

The measured emission profile of the IR-808 dye and the absorption profile of $Nd^{3+}$ or $Yb^{3+}$ ions are presented in Figure S41. According to equation S7, the overlap *J* value is calculated to be *J= 3.732 e+12* ($nm^4$/M cm) between the IR-808 dye and the $Nd^{3+}$ ions, and to be *J= 8.319e+11* ($nm^4$/M cm) between the IR-808 dye and the $Yb^{3+}$ ions. As a result, following equation S6, the Förster radius $R_0$ was calculated to be 1.9 nm when the $Nd^{3+}$ is utilized as the energy acceptor, and 1.49 nm when the $Yb^{3+}$ ions are utilized as the energy acceptor. Moreover, for equation S5, the natural lifetime of the energy donor of the IR-808 dye in its singlet state was evaluated using the formula:

$$1/\tau_D = (1/1.5003)\cdot f \cdot E^2 \qquad \text{(S9)}$$

where *f* is the oscillator strength and *E* is the energy (in $cm^{-1}$) of the vertical electronic transition.

The dependence of efficiency of energy transfer from the IR-808 dye to $Nd^{3+}$ or $Yb^{3+}$ ions versus the donor-acceptor distance is presented in Figure S37, along with the efficiency ratio of $ET_{Dye\text{-}Nd}$/ $ET_{Dye\text{-}Yb.}$ The rates of energy transfer from the IR-808 dye to $Nd^{3+}$ or $Yb^{3+}$ versus the distance between them is presented in Figure S38 which also includes the energy transfer rate ratio of $R_{Dye\text{-}Nd}/R_{Dye\text{-}Yb.}$ The efficiency for energy transfer from IR-808 dye to $Nd^{3+}$ is ~ 2-4 times higher than that for energy transfer from IR-808 dye to $Yb^{3+}$ when the donor-acceptor distance is larger than 1.5 nm, while the efficiencies for both energy transfers are close to 100% when the

donor-acceptor distance is less than 1 nm (Figure S42). The energy transfer rate for IR-808 dye→$Nd^{3+}$ is ~4.3 times higher than the one for IR-808 dye→$Yb^{3+}$ in all the range of distance (Figure S38). The efficiency for IR-808 dye→$Nd^{3+}$ energy transfer was experimentally determined to be ~82%, which corresponds to a donor-acceptor distance of ~ 1.52 nm, commensurate with the linear length scale of the IR-808 dye (~ 2 nm). These results indicate that the IR-808 dye has to be placed closely to the nanoparticle surface to evoke an efficient dye-sensitization effect.

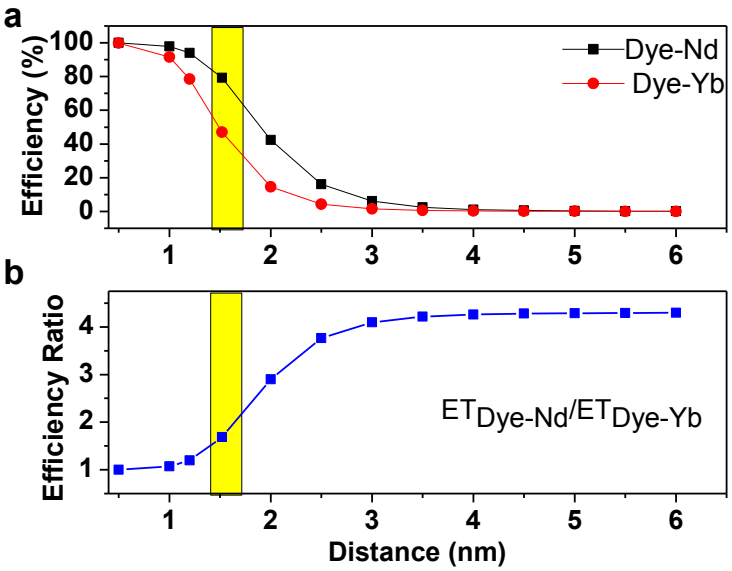


**Figure S42.** (a) The dependence of efficiencies of energy transfers from IR-808 dye to $Nd^{3+}$ or $Yb^{3+}$ on the distance between them; (b) The ratio between the efficiency for energy transfer from IR-808 dye to $Nd^{3+}$ and the efficiency for energy transfer from IR-808 dye to $Yb^{3+}$ versus the donor-acceptor distance. The distances between the IR-808 dye and $Nd^{3+}$ and the IR-808 dye and $Yb^{3+}$ are set to be equal. The results are highlighted in yellow at the estimated real donor-acceptor distance of ~ 1.52 nm.

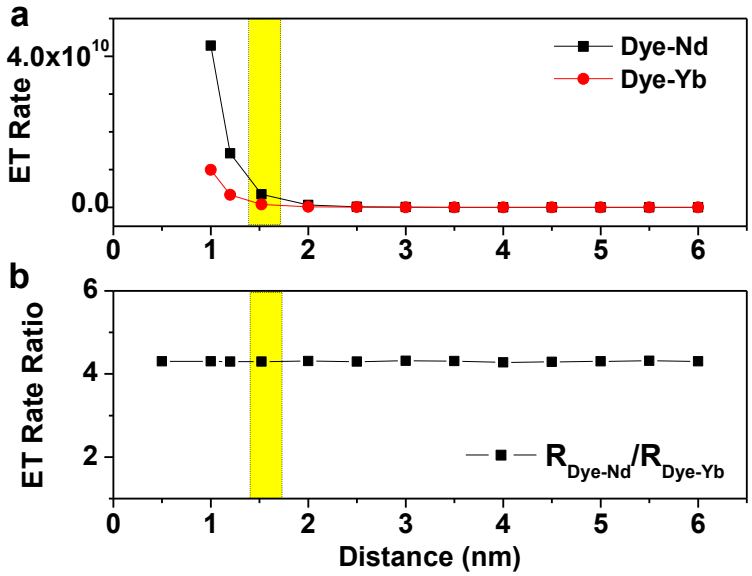


**Figure S43.** (a) The dependence of rates of energy transfers from the IR-808 dye to $Nd^{3+}$ or $Yb^{3+}$ on the distance between them; (b) The ratio between the rate for energy transfer from IR-808 dye to $Nd^{3+}$ and the efficiency for energy transfer from IR-808 dye to $Yb^{3+}$ versus the donor-acceptor distance. The distances between the IR-808 dye and $Nd^{3+}$ and the IR-808 dye and $Yb^{3+}$ are set to be equal. The results are highlighted in yellow at the estimated real donor-acceptor distance of ~ 1.52 nm.

## 2. Evaluation of Efficiency and Rate for the $Nd^{3+}\rightarrow Yb^{3+}$ Energy Transfer.

The emission spectrum of $Nd^{3+}$ ions and the absorption spectrum of $Yb^{3+}$ ions typically have very limited spectral overlap due to the nature of non-resonant energy transfer, rendering the spectral overlap integral J rather small.[16,17] However, an efficient energy transfer from $Nd^{3+}$ to$Yb^{3+}$ has usually been observed because of the significant involvement of multiple phonons from the host lattice to efficiently bridge the energy difference associated with the energy transfer.[18] A complicated and careful consideration of the phonon density of the host lattice has to be implemented to produce a phonon modified spectral overlap integral in order to estimate the J value as well as the Förster radius $R_0$.[17] To avoid a complicated theoretical treatment, instead, we utilized experimentally determined values of the efficiency (~80%) for the $Nd^{3+}$-$Yb^{3+}$ energy transfer and the real distance between the $Nd^{3+}$ and $Yb^{3+}$ ions (the length of c-axis of a unit cell, ~ 0.353 nm) to retrieve the Förster radius $R_0$ according to equation S8. We estimated the Förster radius $R_0$ to be ~ 0.45 nm and $k_{Nd\text{-}Yb}$ to be ~ 3.6 $10^4$ $s^{-1}$ using the reported lifetime of 240 μs for the $^4F_{3/2}$ state of $Nd^{3+}$.[3]

## 3. Evaluation of Energy Transfer Efficiency of IR-808 dye$\rightarrow Nd^{3+}\rightarrow Yb^{3+}$ and IR-808 dye$\rightarrow Yb^{3+}$.

Combining the energy transfer efficiency results in J1 section 1 and 2, we are able to estimate the allover efficiency of the multistep cascade energy transfer route, i.e., IR-808 dye$\rightarrow Nd^{3+}\rightarrow Yb^{3+}$ according to the formula,

$E_{total}=E_1\times E_2$ (S10)

where $E_1$ is the energy transfer efficiency of IR-808 dye→$Nd^{3+}$, and $E_2$ is the one of $Nd^{3+}$→$Yb^{3+}$. The result is presented in Figure S44, in comparison with the efficiency of the direct energy transfer route (from IR-808 dye to $Yb^{3+}$ ions). As one can see, the efficiency for the energy transfer rate mediated by $Nd^{3+}$ ions is ~ 1.5-3.5 times higher than that for the direct energy transfer route from the IR-808 dye to $Yb^{3+}$ ions over almost the entire range of distances (from 1.5 to 6 nm). At the estimated real distance of 1.52 nm between the donor and the acceptor, the energy transfer efficiency for the route IR-808 dye→$Nd^{3+}$→$Yb^{3+}$ can be ~ 1.5 times higher than that for the route IR-808 →$Yb^{3+}$.

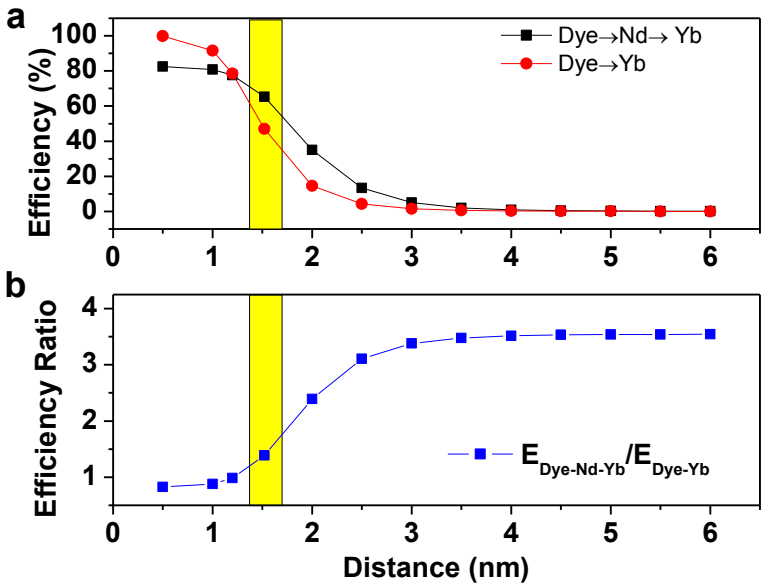


**Figure S44.** (a) The dependence of efficiencies for the energy transfer routes of IR-808 dye→$Nd^{3+}$→$Yb^{3+}$ and IR-808 dye→$Yb^{3+}$, on the distance between them; (b) The ratio between the energy transfer efficiency for the route of dye→$Nd^{3+}$→$Yb^{3+}$ and the route of IR-808 dye→$Yb^{3+}$ versus the distance between the IR-808 dye and $Nd^{3+}$ (or $Yb^{3+}$). The distances between the IR-808 dye and $Nd^{3+}$ and the IR-808 dye and $Yb^{3+}$ are set to be equal. The results are highlighted in yellow at the estimated real donor-acceptor distance of ~ 1.52 nm.

## J2. The Rate Equation Model

The energy transfer occurs from the first singlet excited state of dye (12500 $cm^{-1}$) to $^4F_{5/2}$ of $Nd^{3+}$ (12330 $cm^{-1}$). After the transfer, phonon assisted relaxation occurs from $^4F_{5/2}$ to $^4F_{3/2}$ (11290 $cm^{-1}$) which is not a forbidden transition in the non-symmetric inorganic environment due to the crystal field effect. Further, energy transfer occurs then from $^4F_{3/2}$ to $^2F_{5/2}$ (10300 $cm^{-1}$) in the $Yb^{3+}$ ions. The last step is the upconversion to the $Tm^{3+}$ ions. The scheme of energy transfer with all energy channels is illustrated on Fig. S45.

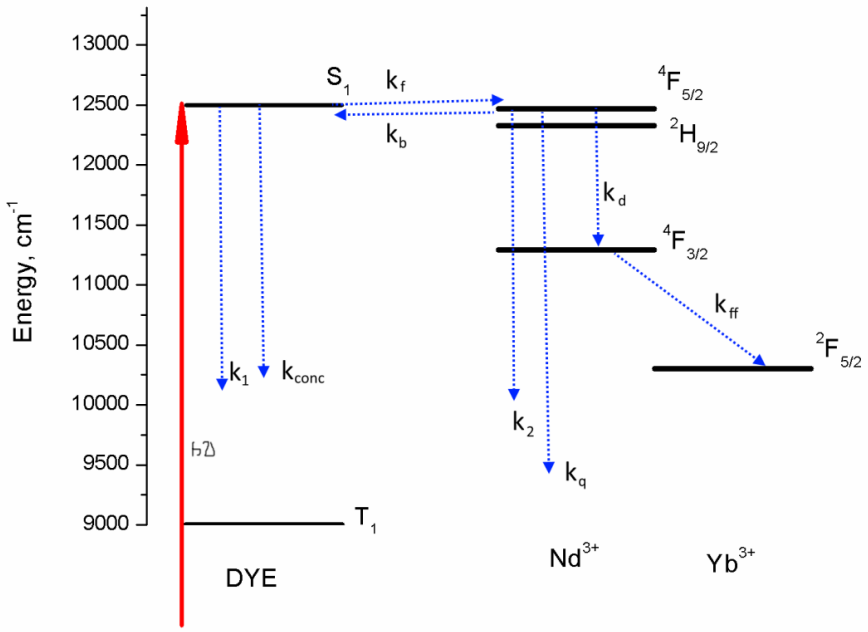


**Figure S45.** The scheme of energy transfer

In Fig. S45, $h\nu$ is excitation of dye (D), $k_1$ is radiative and nonradiative deexcitation of D, $k_{conc}$ is the concentration quenching of D in the process of $D^*+D \xrightarrow{k_{conc}} D+D$, where $D^*$ is the dye in the first excited singlet state. This process may include either formation of excimers that cannot transfer energy to $Nd^{3+}$ (Nd) or cross-relaxation of the excited dye with energy migration out of the reaction zone. Other values: $k_f$ is pumping rate for the $^4F_{5/2}$ state of $Nd^{3+}$, $k_b$ is back energy transfer rate from the $^4F_{5/2}$ state of $Nd^{3+}$, $k_2$ is radiative and nonradiative deexcitation of Nd, $k_q$ is concentration quenching rate of Nd in the process of $Nd^*+Nd \xrightarrow{k_q} Nd+Nd$, where $Nd^*$ is the number of Nd in the $^4F_{5/2}$ state; $k_d$ is non-radiative relaxation rate to $^4F_{3/2}$ and $k_{ff}$ is energy transfer rate to the $^2F_{5/2}$ state of $Yb^{3+}$.

We apply the rate equation model for the energy transfer from the environment to $Ln^{3+}$ ion.[19] We consider the following processes involving the dye and $Nd^{3+}$.

1. $D \xrightarrow{h\nu} D^*$ (excitation of D)
2. $D^* \xrightarrow{k_1} D$ (radiative and nonradiative deexcitation of D)
3. $D^*+D \xrightarrow{k_{conc}} D+D$ (concentration quenching of D).
4. $D^*+Nd \xrightarrow{k_f} Nd^*+D$ (pumping the $^4F_{5/2}$ state of $Nd^{3+}$)
5. $Nd^*+D \xrightarrow[k_b]{} D^*+Nd$ (back energy transfer from $^4F_{5/2}$ state of $Nd^{3+}$)
6. $Nd^* \xrightarrow{k_2} Nd$ (radiative and nonradiative deexcitation of Nd)

7. $Nd^* + Nd \xrightarrow{k_q} Nd + Nd$ (concentration quenching of Nd).

Let $D$ and $D^*$ be the instantaneous concentrations of the dye molecules in the ground and excited state, and $Nd$ and $Nd^*$ be the instantaneous concentrations of $Nd^{3+}$ in the ground ($^4I_{9/2}$) and excited ($^4F_{5/2}$) states, respectively. The assumptions and approximations made in literature are valid also for the system in study.[19] The total dye concentration is $D_0 = D + D^*$; but at low irradiation intensity, $D^*$ is a small fraction of $D_0$, and $D \approx D_0$. The same is true for Nd: $Nd^*$ is a small fraction of the total $Nd$ concentration $Nd_0$, and $Nd \approx Nd_0$.

The rate of the excitation under continuous irradiation is just the probability $w$ of the electronic transition per unit time; the rate $r_e$ of this process is

$$r_e = wD,$$

The rate $r_d$ of the deexcitation process is

$$r_1 = k_1 D^*$$

The rate $r_{conc}$ of the concentration quenching is

$$r_{conc} = k_{conc} D \cdot D^*$$

The rates of the forward $r_f$ and backward $r_b$ energy transfer are

$r_f = k_f D^* \cdot Nd$ and $r_b = k_b D \cdot Nd^*$.

So the total rate with respect to the intermediate D* is

$$\frac{dD^*}{dt} = wD + k_b D \cdot Nd^* - (k_1 + k_f Nd + k_{conc} D) \cdot D^* \qquad \text{(S11)}$$

Nd* is produced through the energy transfer from D* with the rate

$$r_f = k_f D^* \cdot Nd$$

and consumed through the deexcitation (including energy transfer to $Yb^{3+}$)

$$r_2 = k_2 Nd^*,$$

concentration quenching

$$r_q = k_q Nd \cdot Nd^*,$$

and backward energy transfer

$$r_b = k_b D \cdot Nd^*$$

The total rate with respect to Nd* is

$$\frac{dNd^*}{dt} = k_f D^* \cdot Nd - (k_2 + k_q Nd + k_b D) \cdot Nd^* \qquad \text{(S12)}$$

In the quasi-steady approximation, which is valid for continuous irradiation, $\frac{dD^*}{dt} = 0$ and $\frac{dNd^*}{dt} = 0$. Therefore,

$$Nd^* = \frac{k_f Nd \cdot D^*}{k_2 + k_b D + k_q Nd} \tag{S13}$$

$$D^* = \frac{wD + k_b D \cdot Nd^*}{k_1 + k_f Nd + k_{conc} D}. \tag{S14}$$

After substituting the expression of $Nd^*$ in equation S13 into equation S14, we obtain

$$D^* = \frac{d_1 D^2 + e_1 D}{a_1 D^2 + b_1 D + c_1}, \tag{S15}$$

where $a_1 = k_b k_{conc}$ ; $b_1 = k_1 k_b + k_2 k_{conc} + k_q k_{conc} Nd$ ; $c_1 = k_1 k_2 + k_1 k_q Nd + k_2 k_f Nd + k_q k_f Nd^2$ ; $d_1 = w k_b$ ; $e_1 = w k_2 + w k_q Nd$

The UCL intensities from $^1I_6$, $^1D_2$, $^1G_4$ of $Tm^{3+}$ in Fig. 3b depend on the D* concentration (the excited states of D and Nd). Therefore we carried out a fitting procedure of the expression in equation S15 using the method of least squares (Maple software),[20] and a linear relation between the intensity of $^1I_6$, $^1D_2$, $^1G_4$ of $Tm^{3+}$ of $Tm^{3+}$ and the D* concentration in the following

$$I = k*C + B \tag{S16}$$

where $k$, $B$ are constant and C is $D^*$, $I$ is the intensity of the UCL from $^1I_6$, $^1D_2$, $^1G_4$ of $Tm^{3+}$. Equation S16 is validated sufficiently in our case, as the utilized irradiance of 10 W/cm$^2$ in Fig. 3b falls well within an extreme saturation excitation regime where a linear dependence between the UCL intensity and the absorbed excitation energy exists (See Fig. S35).

## K. References


1. Pandozzi, F.; Vetrone, F.; Boyer, J. C.; Naccache, R.; Capobianco, J. A.; Speghini, A.; Bettinelli, M., A spectroscopic analysis of blue and ultraviolet upconverted emissions from $Gd_3Ga_5O_{12}$: $Tm^{3+}$, $Yb^{3+}$ nanocrystals. *J Phys Chem B* **2005,** *109* (37), 17400-17405.

2. Mai, H. X.; Zhang, Y. W.; Si, R.; Yan, Z. G.; Sun, L. D.; You, L. P.; Yan, C. H., High-quality sodium rare-earth fluoride nanocrystals: Controlled synthesis and optical properties. *J Am Chem Soc* **2006,** *128* (19), 6426-6436.

3. Chen, G. Y.; Ohulchanskyy, T. Y.; Liu, S.; Law, W. C.; Wu, F.; Swihart, M. T.; Agren, H.; Prasad, P. N., Core/Shell $NaGdF_4$:$Nd^{3+}$/$NaGdF_4$ Nanocrystals with Efficient Near-Infrared to Near-Infrared Downconversion Photoluminescence for Bioimaging Applications. *ACS nano* **2012,** *6* (4), 2969-2977.

4. Xie, X. J.; Gao, N. Y.; Deng, R. R.; Sun, Q.; Xu, Q. H.; Liu, X. G., Mechanistic Investigation of Photon Upconversion in Nd3+-Sensitized Core-Shell Nanoparticles. *J Am Chem Soc* **2013,** *135* (34), 12608-12611.

5. Zou, W. Q.; Visser, C.; Maduro, J. A.; Pshenichnikov, M. S.; Hummelen, J. C., Broadband dye-sensitized upconversion of near-infrared light. *Nat Photonics* **2012,** *6* (8), 560-564.

6. Dong, A. G.; Ye, X. C.; Chen, J.; Kang, Y. J.; Gordon, T.; Kikkawa, J. M.; Murray, C. B., A Generalized Ligand-Exchange Strategy Enabling Sequential Surface Functionalization of Colloidal Nanocrystals. *J Am Chem Soc* **2011,** *133* (4), 998-1006.

7. Xu, C. T.; Svenmarker, P.; Liu, H. C.; Wu, X.; Messing, M. E.; Wallenberg, L. R.; Andersson-Engels, S., High-Resolution Fluorescence Diffuse Optical Tomography Developed with Nonlinear Upconverting Nanoparticles. *ACS Nano* **2012,** *6* (6), 4788-4795.

8. Sahoo, Y.; Goodarzi, A.; Swihart, M. T.; Ohulchanskyy, T. Y.; Kaur, N.; Furlani, E. P.; Prasad, P. N., Aqueous ferrofluid of magnetite nanoparticles: Fluorescence labeling and magnetophoretic control. *J Phys Chem B* **2005,** *109* (9), 3879-85.

9. Kumar, R.; Roy, I.; Ohulchanskyy, T. Y.; Goswami, L. N.; Bonoiu, A. C.; Bergey, E. J.; Tramposch, K. M.; Maitra, A.; Prasad, P. N., Covalently dye-linked, surface-controlled, and bioconjugated organically modified silica nanoparticles as targeted probes for optical imaging. *ACS nano* **2008,** *2* (3), 449-56.

10. Chen, G. Y.; Shen, J.; Ohulchanskyy, T. Y.; Patel, N. J.; Kutikov, A.; Li, Z. P.; Song, J.; Pandey, R. K.; Agren, H.; Prasad, P. N.; Han, G., (alpha-$NaYbF_4$:$Tm^{3+}$)/$CaF_2$ Core/Shell Nanoparticles with Efficient Near-Infrared to Near-Infrared Upconversion for High-Contrast Deep Tissue Bioimaging. *ACS nano* **2012,** *6* (9), 8280-8287.

11. Ward, M. D., Mechanisms of sensitization of lanthanide(III)-based luminescence in transition metal/lanthanide and anthracene/lanthanide dyads. *Coordin Chem Rev* **2010,** *254* (21-22), 2634-2642.

12. Zhou, J.; Liu, Q.; Feng, W.; Sun, Y.; Li, F. Y., Upconversion Luminescent Materials: Advances and Applications. *Chem Rev* **2015,** *115* (1), 395-465.

13. Suyver, J. F.; Aebischer, A.; Garcia-Revilla, S.; Gerner, P.; Gudel, H. U., Anomalous power dependence of sensitized upconversion luminescence. *Phys Rev B* **2005,** *71* (12).

14. Clegg, R., Förster resonance energy transfer-FRET: what is it, why do it, and how it's done. In *FRET and FLIM Techniques*, Gadella, T. W. J., Ed. Academic Press: Burlington, 2009; Vol. 33, pp 1-57.

15. http://en.wikipedia.org/wiki/F%C3%B6rster_resonance_energy_transfer.

16. Auzel, F., Multiphonon-assisted anti-Stokes and Stokes fluorescence of triply ionized rare-earth ions. *Phys Rev B* **1976,** *13* (7), 2809-2817.

17. Jaque, D.; Ramirez, M. O.; Bausa, L. E.; Sole, J. G.; Cavalli, E.; Speghini, A.; Bettinelli, M., $Nd^{3+}$-> $Yb^{3+}$ energy transfer in the $YAl_3(BO_3)_4$ nonlinear laser crystal. *Phys Rev B* **2003,** *68* (3), 9.

18. Lupei, A.; Lupei, V.; Ikesue, A.; Gheorghe, C.; Hau, S., Nd -> Yb energy transfer in (Nd, Yb):$Y_2O_3$ transparent ceramics. *Opt. Mater.* **2010,** *32* (10), 1333-1336.

19. Meza, O.; Villabona-Leal, E. G.; Diaz-Torres, L. A.; Desirena, H.; Rodriguez-Lopez, J. L.; Perez, E., Luminescence Concentration Quenching Mechanism in $Gd_2O_3$:$Eu^{3+}$. *J Phys Chem A* **2014,** *118* (8), 1390-1396.

20. http://www.maplesoft.com.